Seasonal Amplification and Spatial Reorganization of Atmospheric Ammonia (NH_3) in Northeast China

S1 Observation support and harmonization

The descriptive record contains 464,712 potential cell-month records, of which 464,225 are finite. It retains 60,672 negative retrievals (13.07% of the finite record). Model exclusions apply only to the 2008–2022 mechanism analysis. No missing-value imputation or observation-count threshold was introduced. IASI uncertainty terms remain separate because their covariance and confidence convention were not supplied. The original fractional nobs reflects producer sampling support and is not rounded to an integer count. Fig. S2 and Table S2 document these observations.

ERA5 alignment does not improve the physical resolution of the original 0.25° fields. ERA5-Land uses finite land support, retaining its valid-area fraction. EDGAR mass redistribution used extensive source-cell totals and spherical overlap fractions; integrated conservation checks differed by less than 3.7×10^{-16} relative to direct source sums. MODIS denominator land codes retained classified/corrected/backfilled source labels with valid IGBP classes 1–16, excluding unclassified, water and fill. Static 2020 cropland does not represent historical land-cover change. Provincial weights use actual intersection areas, whereas province indicators use the largest cell overlap.

S2 Descriptive trend and hotspot definitions

The main regional annual series averages area-weighted monthly means with equal temporal weight. An alternative annual series first averages at the cell and then spatially, and observation-support weighting is retained as a sensitivity. These aggregation orders can differ when missingness varies. Table S3 retains Theil–Sen, OLS/HAC and Mann–Kendall outputs and the area evidence summaries. The BH–FDR family is the set of finite annual cell-trend tests across NE3. Regional Theil–Sen uncertainty was also assessed by two- and three-year circular moving-block resampling of detrended annual residuals (1,999 replicates). For field significance, cell-wise detrended residuals were resampled with common temporal blocks across all grid cells to preserve coherent interannual spatial variability; observed positive-trend area was compared with the no-trend null distribution (Table S6).

Relative hotspot thresholds are area-weighted inverse empirical-CDF percentiles of each year's cell annual NH_3, with strict exceedance retaining tied values. Realized hotspot area can therefore differ slightly from 10%. Persistence ≥0.8 means at least 14 of the 17 years. The fixed P90 sensitivity uses a single threshold from the temporal mean of annual cell columns. Centroid weights include excess above the relevant threshold, so movement describes changing intensity and configuration. Table S9 retains signed displacement components, persistence, provincial shares and alternative definitions. Fig. S6 and Table S7 retain all seasonal definitions. Annual centroid-coordinate trends were estimated with separate Theil–Sen slopes for projected east and north coordinates (EPSG:6933). Paired two- and three-year circular moving-block bootstrap resampling of detrended coordinate residuals (1,999 replicates) provided uncertainty checks; trends were also evaluated excluding 2008 and under alternative hotspot thresholds (Table S10).

S3 Interpretation and uncertainty

The frozen UST-BART ensemble retained fifty grow-from-root samples for each of two seeds. Response curves pool these samples equally after calculating local effects independently for each sample. At most 96 observed reference rows per bin supplied first-order ALE; province curves used at most 72. Local response differences were integrated and centred by bin counts. Confidence intervals for Theil–Sen trends and approximate forest-response bands for model responses refer to different estimands.

Curve ordinates are forest medians. The already-frozen endpoint contrasts, province response changes, relevance shares and interaction mixed contrasts are forest-mean summaries. For example, the pooled median-curve endpoint difference for regional temperature is 86.6 μmol m^{-2}, whereas the reported mean endpoint

contrast is 84.5 μmol m^{-2}. This numerical difference follows the summary functional and does not indicate a different model. Approximate forest-response bands are the pooled 2.5th and 97.5th percentiles of the corresponding sample responses. They do not include retrieval-error propagation or prediction-error noise.

Turning patterns were detected with 20% of curve-amplitude prominence and at least two-bin separation; corresponding major turns were compared within 15% of grid length. Shape correlation alone did not establish stability. First-order curves and local interaction contrasts remain conditional on the observed predictor context and support. Correlated inventory and land-use variables can share predictive information. Model relevance is split use, and a weak between-driver relevance share does not imply that geography is unimportant because spatial adjustment is also present.

S4 Validation and complementary mechanism results

The UST-BART temporal test is a conditional hindcast with a static 2020 cropland background. Predictor means for that test were derived from 2008–2018 only. The spatial test region is a continuous eastern strip covering Jilin and Heilongjiang; its metrics do not directly validate extrapolation to Liaoning. Table S16 reports residual bias by month and province and residual Moran's I. Fig. 6 is a fitted descriptive comparison on matched model rows, rather than a third independent validation. An undecomposed XBART comparator, using the same holdouts and GFR settings, tests the predictor decomposition directly (Table S17).

Complete driver relevance and all fifteen physical response curves are preserved in Table S12, Table S13, Fig. S9 and Fig. S10. All 105 interaction pairs are preserved in Table S14 and Fig. S11, including lower-support and unstable results. The two temperature interactions in the main text had twenty-five supported grid cells each. Supplementary agricultural background interactions were less reproducible and are shown as screening evidence in Fig. S12. Province differences in moisture, BLH and annual AGS responses are summarized over common support in Fig. S13 and Table S15.

S5 Additional revision checks

Low-support records were evaluated with the producer's fractional nobs ≥0.25 sensitivity, without rounding counts. The regional/monthly distributions and same-period response selection comparisons accompany the added figures and tables. Recomputed held-out metrics and the fixed-seed background-only comparison appear in Table S16. Saved-sample half comparisons and paired province contrasts are in Table S19. Approximate forest-response bands summarize fitted-function variability and exclude observational noise; their reproducibility does not establish calibrated posterior coverage.

All 204 AM monthly subsets were extracted from the official version 4.0.1R MERGED archive on its native 0.2° grid. The first-month archived AM+PM values exactly reproduce the local subset. Monthly source attributes identify Metop-A (2008–2013), Metop-B (2014–2019) and Metop-C (2020–2024). With identical administrative overlap weights and equal-month annual aggregation, NE3 AM/AM+PM slopes are $4.7934097193/4.5240646570 \times 10^{-5}$ mol m^{-2} $decade^{-1}$, and Early-to-Late amplitude increases are 119.7795/119.6848%. Both preserve Liaoning > Jilin > Heilongjiang trend ordering. The support ≥0.25 sensitivity gives AM/AM+PM slopes $4.7703288841/4.5269961909 \times 10^{-5}$ and amplitude increases 120.2426/119.4598%. AM+PM has 1,676 low-support records among 464,712 grid-month support records (0.3607%), concentrated in January (620 records) and February (279). Area-time weighted negative fractions are 15.6400% for AM and 12.6847% for AM+PM before filtering. These are signed retrievals, not necessarily invalid measurements. The descriptive comparisons support retaining AM+PM, while PM noise and retrieval sensitivity remain limitations. No AM mechanism refit or observation-interval calibration is claimed.

Further instrument-transition checks compared contemporaneous Metop-A/B (2014) and Metop-B/C (2020) fields on common finite grid cells. Same-instrument bridging, period-specific trends and amplitudes, seasonally adjusted change-point tests and a monthly overlap-offset sensitivity scenario are reported in Table S8. The offsets were used only for sensitivity assessment; the main MERGED record was unchanged.

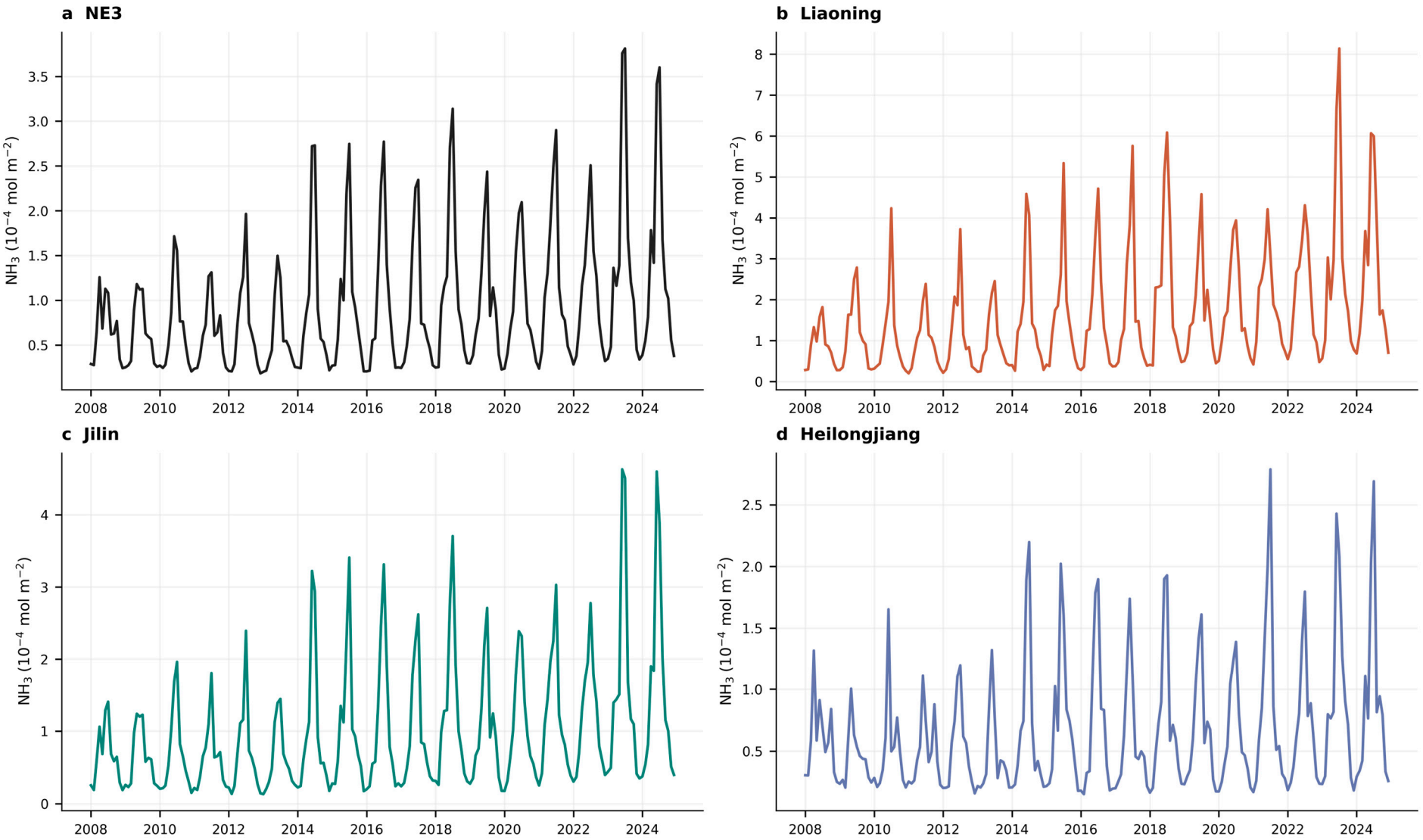


Figure S1. Complete area-weighted monthly IASI NH_3 series, January 2008–December 2024, for (a) NE3, (b) Liaoning, (c) Jilin and (d) Heilongjiang. Finite negative retrievals are retained. NH_3 units are 10^{-4} mol m^{-2}; lines join monthly means without uncertainty bands.

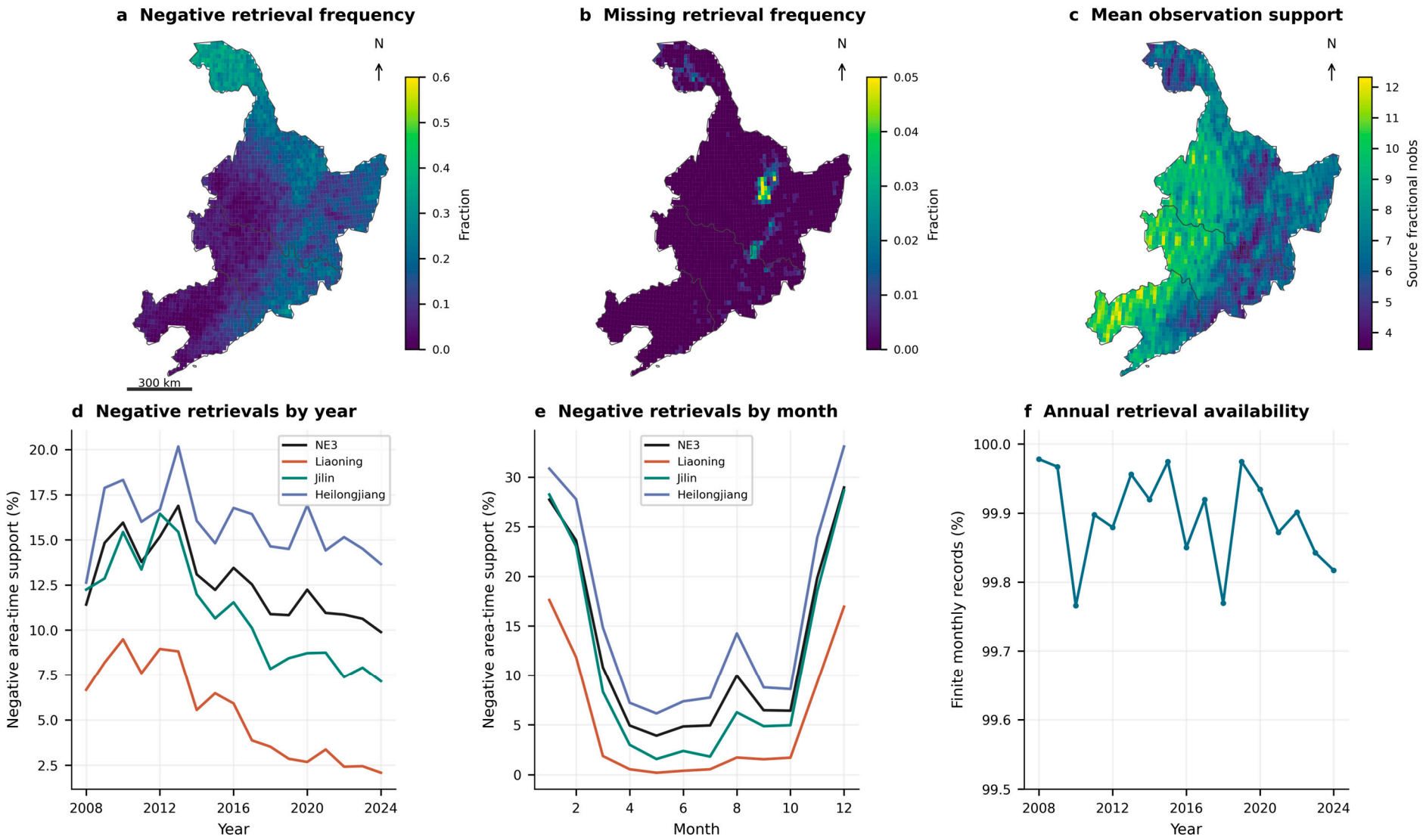


Figure S2. Retrieval support and descriptive preprocessing. (a) Frequency of finite negative retrievals, (b) fraction of missing monthly retrievals, and (c) mean producer-supplied fractional observation support. (d, e) Area-time-weighted negative frequency by year and month. (f) Annual fraction of finite NH_3 cell-month records. Negative and missing values retain separate definitions; source nobs is not an independent integer sample count. Projection follows Fig. 2. Observation diagnostics cover 2008–2024. Map frequencies are fractions; year/month negative frequencies and annual availability are percentages. Observation support is the producer's fractional count. Lines join the corresponding weighted summaries.

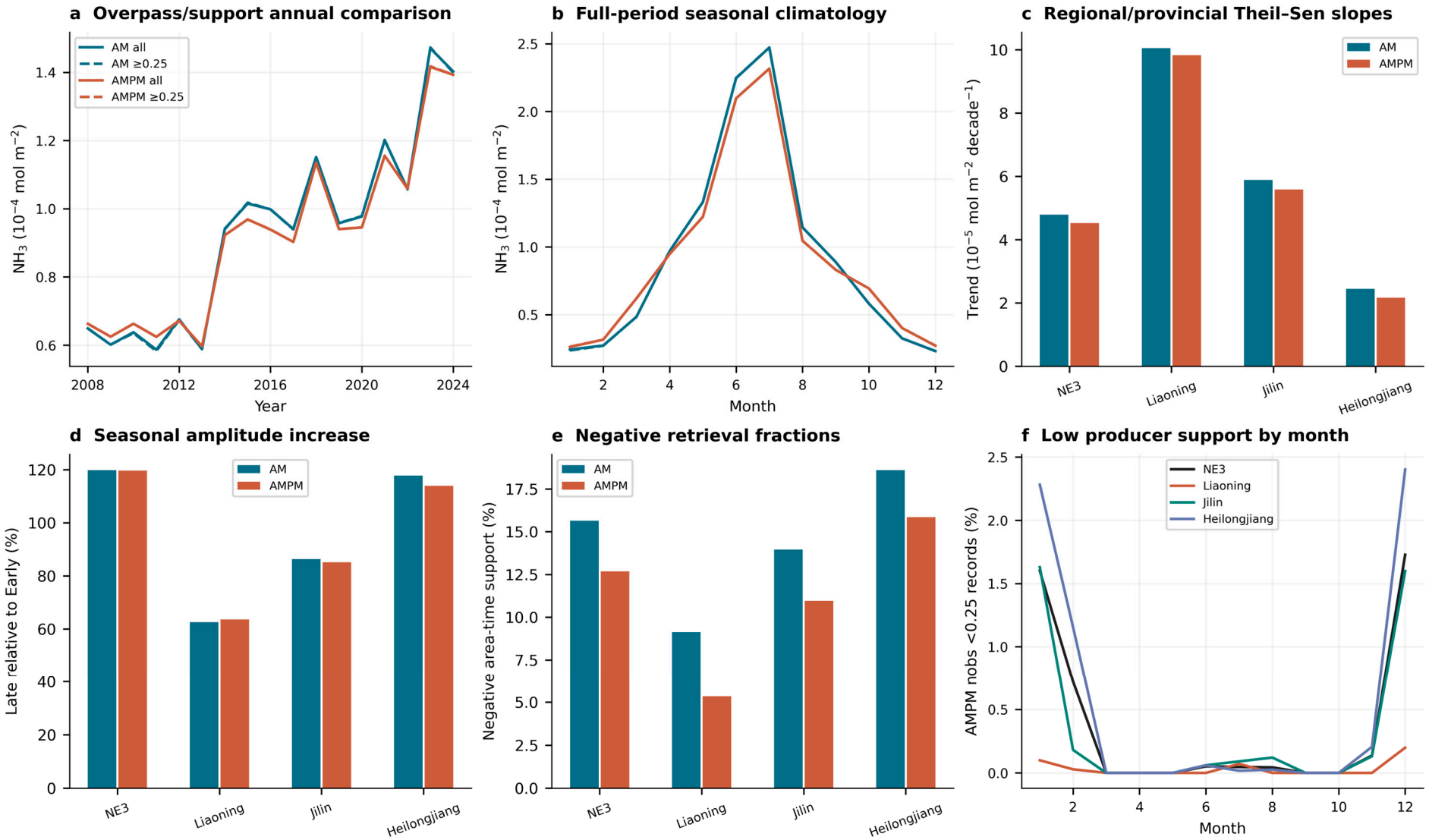


Figure S3. AM versus AM+PM and observation-support sensitivity, 2008–2024. (a) NE3 annual area-weighted columns for AM and AM+PM, each with and without producer support ≥0.25. (b) NE3 calendar-month climatologies on the same spatial weights. (c) Theil–Sen slopes for NE3 and each province. (d) Early-to-Late climatological amplitude changes. (e) Area-time weighted negative retrieval fractions. (f) Low-support monthly record prevalence in the frozen AM+PM record. Units are in Table S1; unrounded values are retained in the accompanying CSV files. These comparisons do not calibrate retrieval uncertainty.

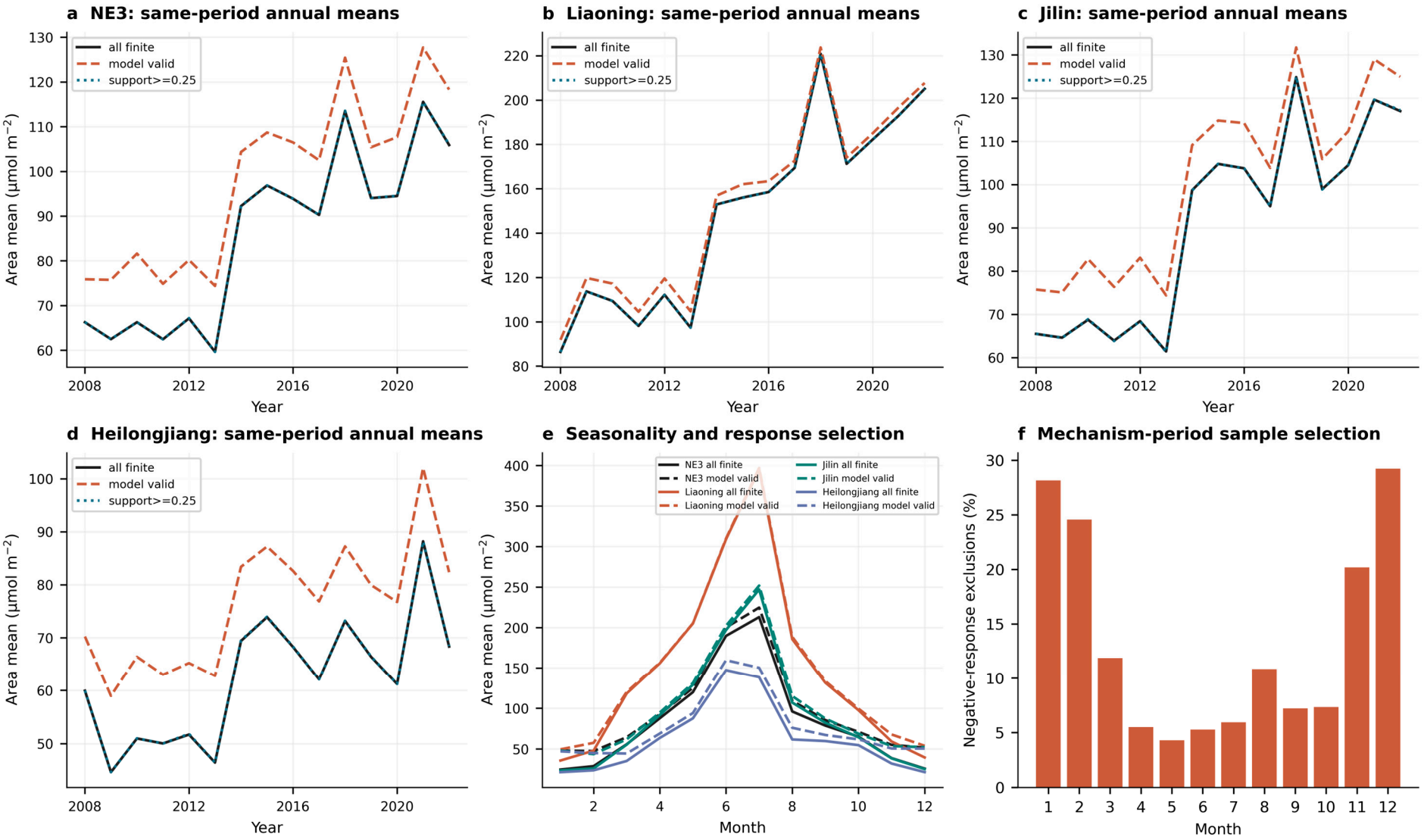


Figure S4. Response-selection sensitivity on common 2008–2022 support. (a–d) Annual area-weighted means for all finite signed retrievals, the frozen nonnegative complete model subset, and the support ≥0.25 sensitivity. (e) Corresponding all-finite versus model-valid monthly climatologies. (f) Fraction of candidate mechanism records excluded for negative response, by month. Region summaries use administrative overlap-area weights; counts and province assignments in Table S4 have separate row-level denominators. Response units are μmol m^{-2}.

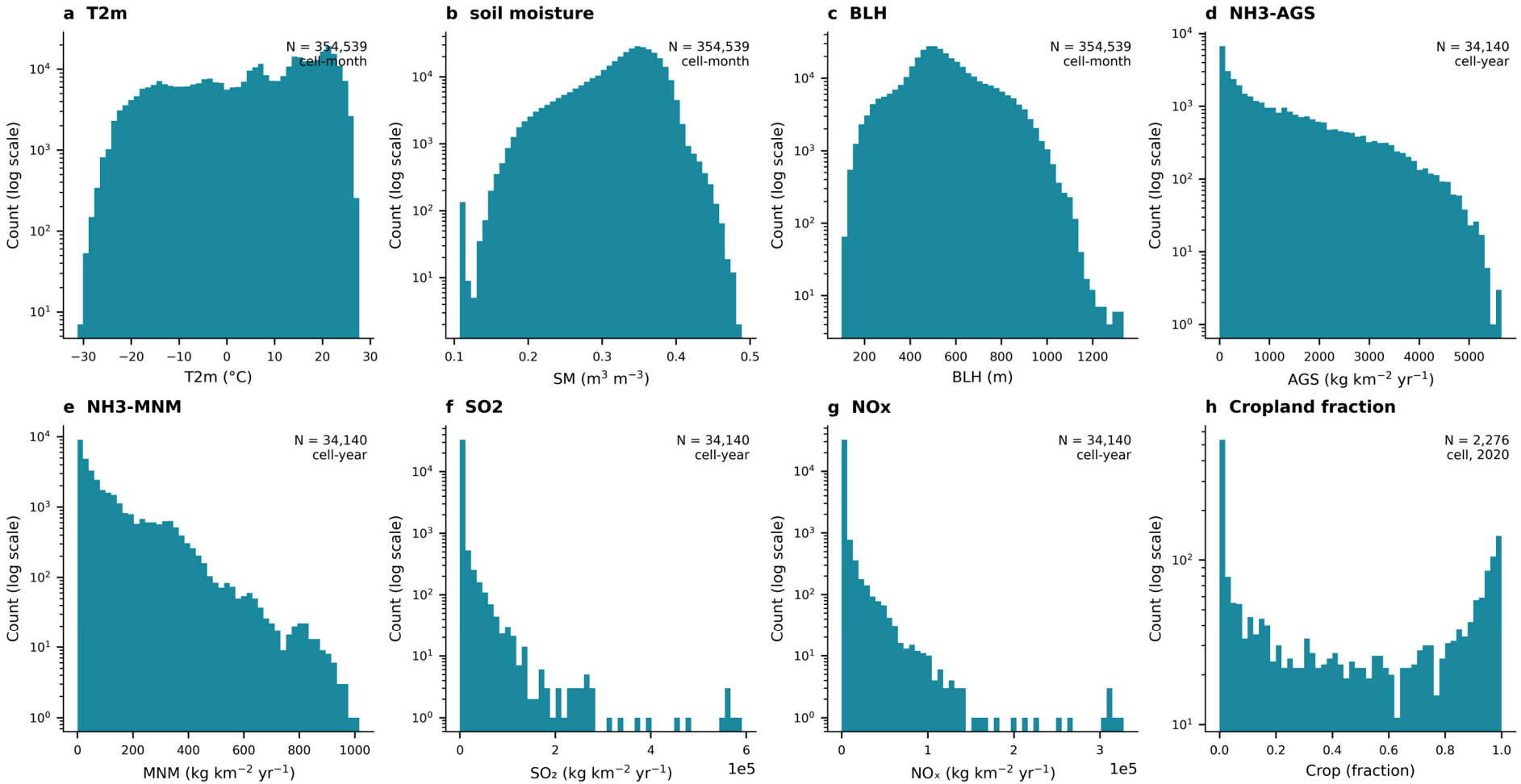


Figure S5. Distributions of the eight physical drivers on valid model support, 2008–2022. Meteorology uses 354,539 cell-months; each inventory uses 34,140 unique cell-years; static 2020 cropland uses 2,276 locations. Predictor values retain original units, before between/within decomposition. Full min–max ranges are shown, with logarithmic count axes to expose high-value tails. Repeated within-year inventories and repeated static values are not counted as independent observations. Descriptive statistics are in Table S5.

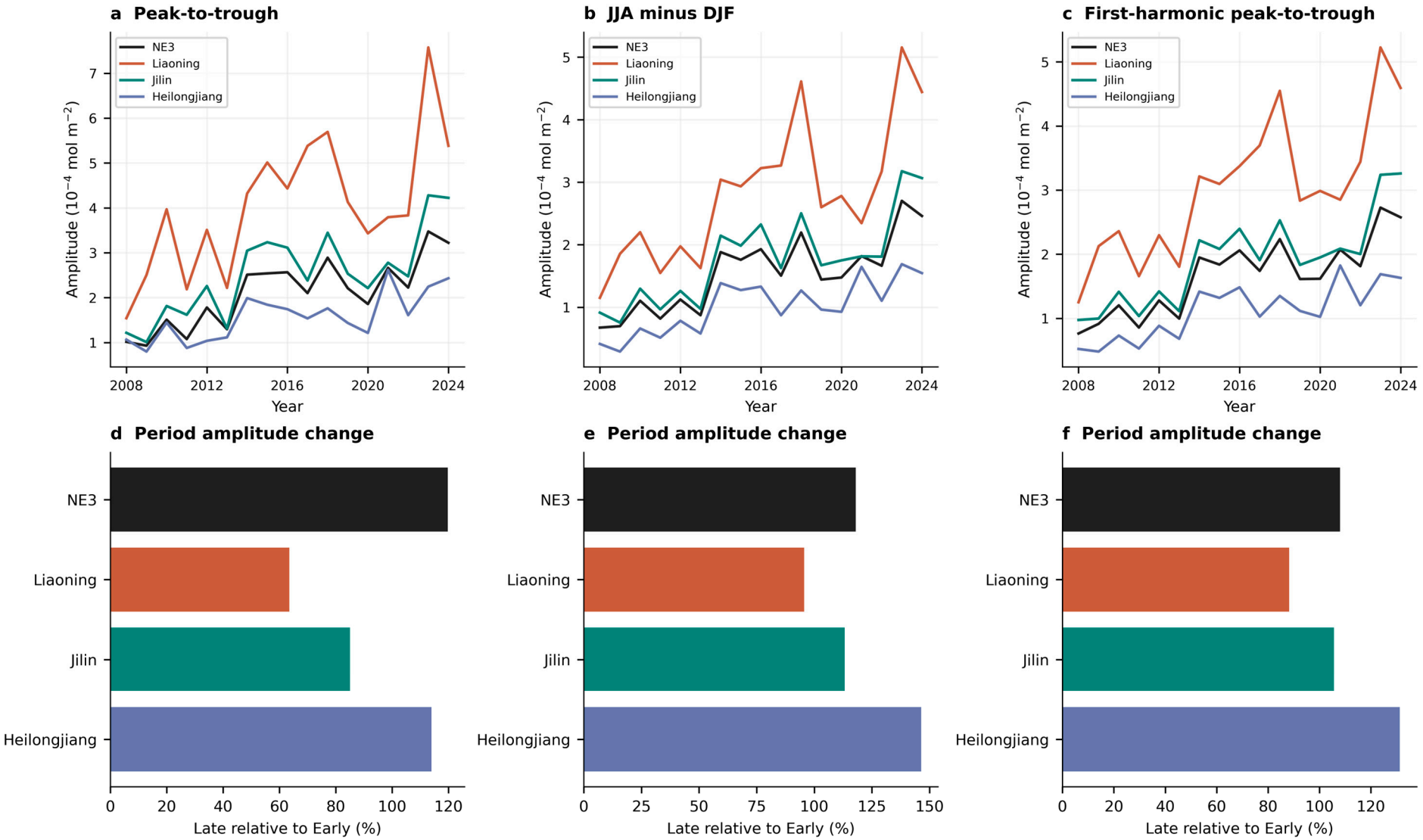


Figure S6. Seasonality sensitivities. Annual regional values for (a) maximum-minus-minimum, (b) JJA-minus-DJF and (c) first-harmonic peak-to-trough amplitude. (d–f) Corresponding percentage changes from Early to Late climatologies, with identical regional colours. Observation diagnostics cover 2008–2024. Amplitude units are 10^{-4} mol m^{-2}; bars give dimensionless percentage change. Lines join annual values without uncertainty bands.

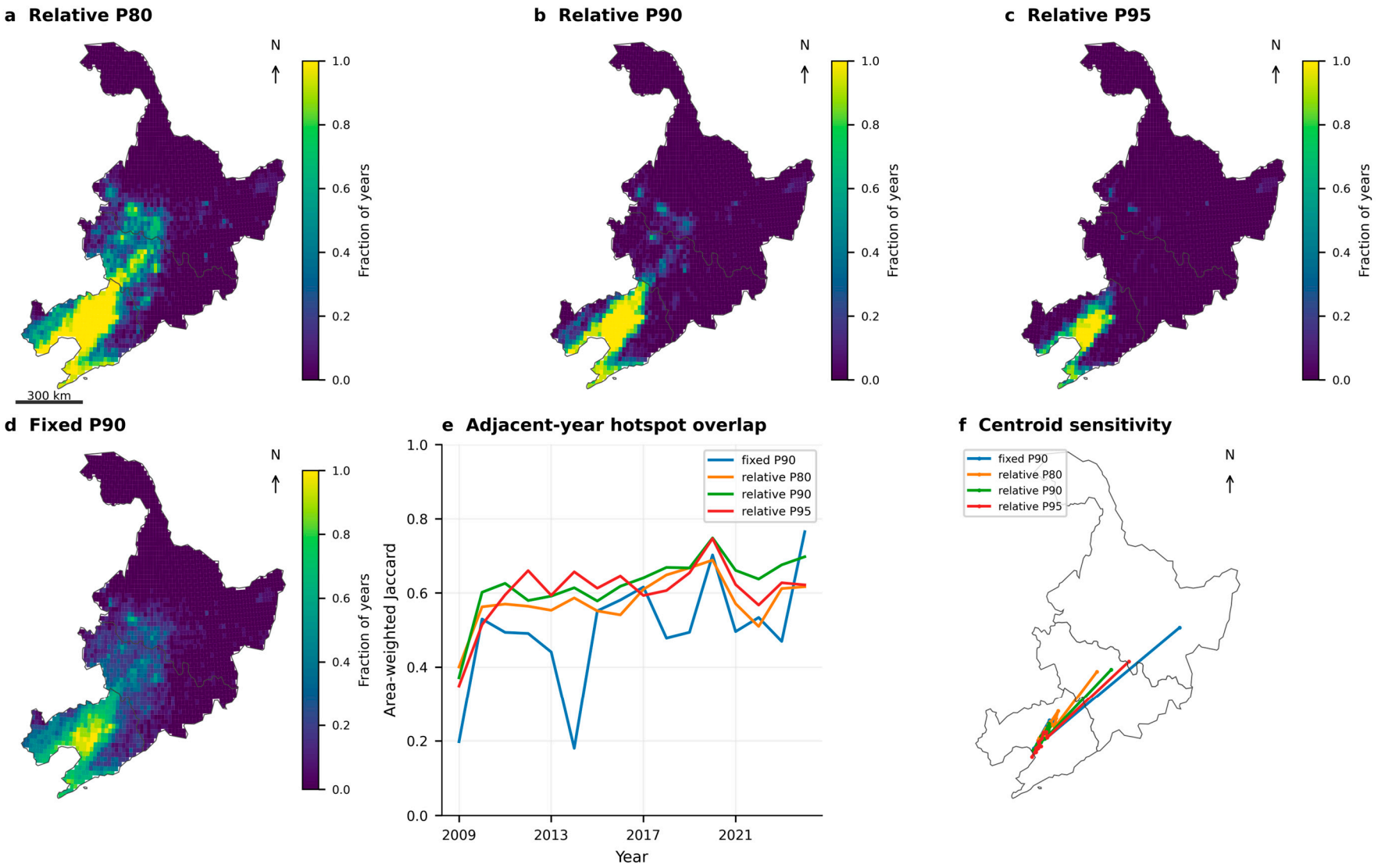


Figure S7. Hotspot-definition sensitivity. Persistence under annual relative (a) P80, (b) P90 and (c) P95 thresholds and (d) the fixed P90 threshold of full-period cell annual means. (e) Area-weighted adjacent-year Jaccard similarity. (f) Excess-weighted annual centroid trajectories for each definition. Projection follows Fig. 2. Observation diagnostics cover 2008–2024. Persistence and Jaccard values are dimensionless. Lines join annual overlap values or centroid coordinates; map projection and scale follow Fig. 2.

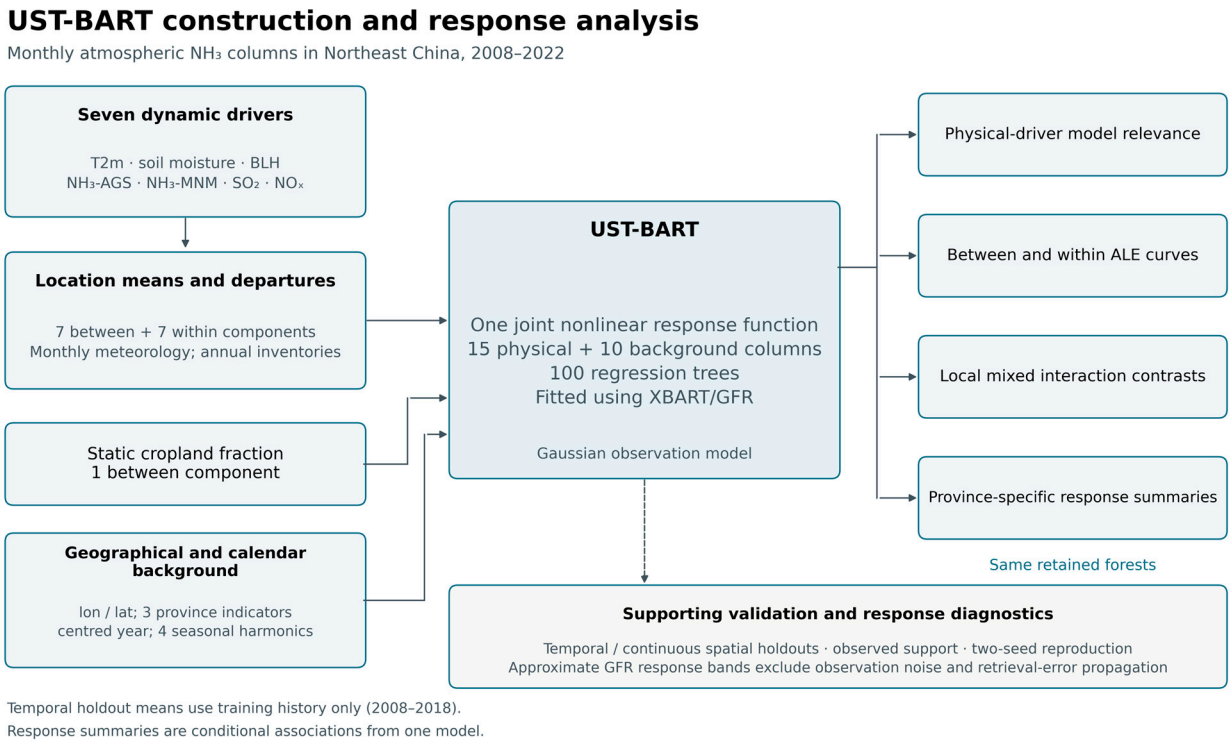


Figure S8. Construction and response analysis of Unified Spatiotemporal Bayesian Additive Regression Trees (UST-BART). Seven dynamic drivers supply seven location means and seven departures; static cropland supplies one between component. Longitude, latitude, three province indicators, centred year and four seasonal harmonic columns add ten background inputs. All 25 columns enter one 100-tree nonlinear response function, fitted using the established XBART/GFR procedure. Relevance, first-order ALE, local mixed contrasts and province-specific summaries use the same retained forests. For temporal testing, location means use 2008–2018 history and are retained for 2019–2022. Meteorological departures vary monthly and retain seasonality; inventory departures vary annually. Supporting diagnostics use the existing temporal and continuous spatial holdouts, observed data support and two-seed comparisons. Approximate GFR forest-response bands exclude observation noise and retrieval-error propagation. Arrows describe analysis flow rather than causal paths; the diagram introduces no additional model fitting or latent spatial process.

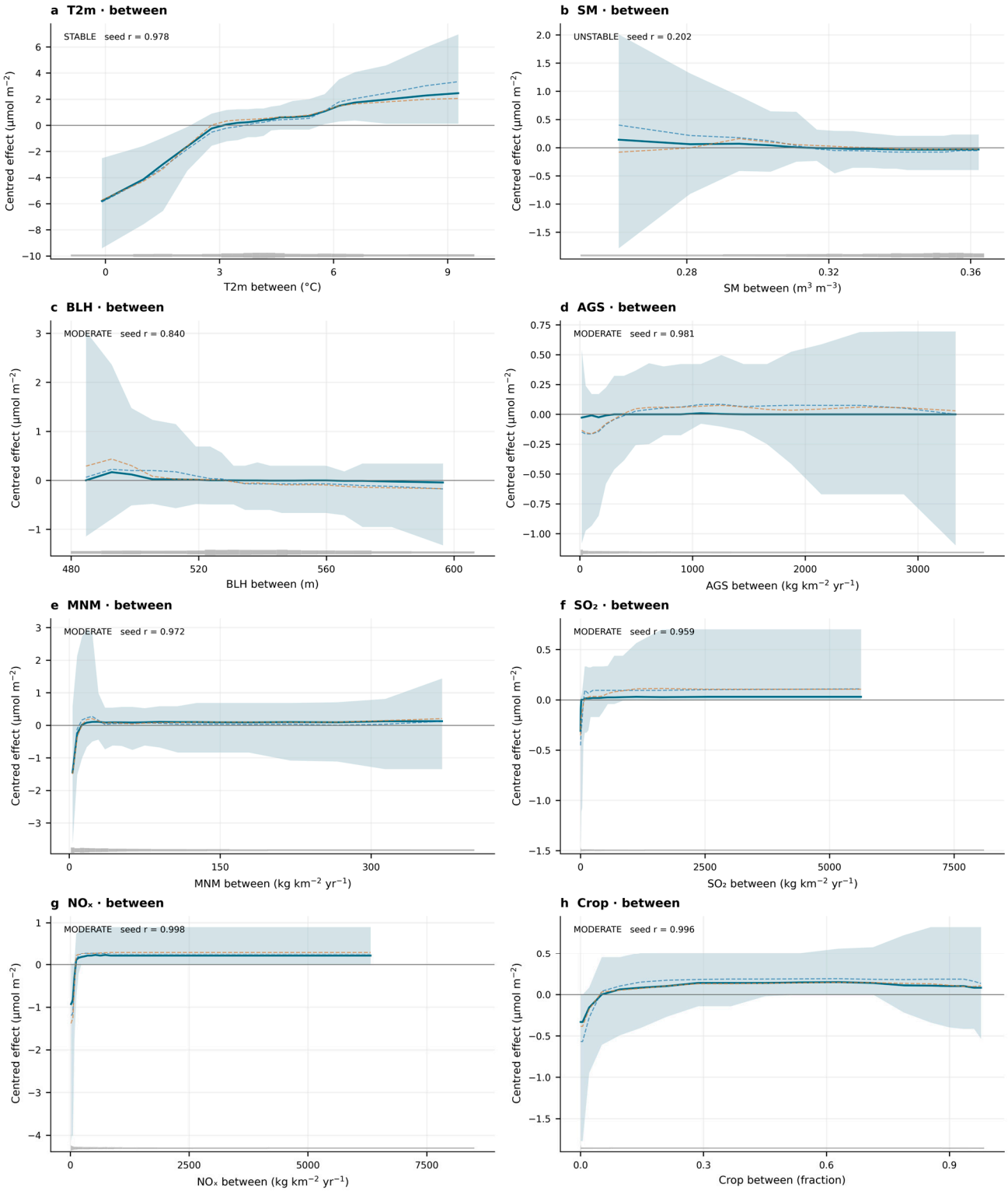


Figure S9. All eight between-location physical-driver ALE curves over P5–P95. Solid lines are pooled forest medians, shading denotes approximate 95% forest-response bands, and dashed lines show the two seeds' forest means. Bottom strips indicate local data density. Shape correlations and stability labels are displayed; unstable curves are retained here for completeness and are not used as principal mechanism evidence. Effect estimates use 2008–2022. Panels (a–h) show T2m, SM, BLH, AGS, MNM, SO_2, NO_x and cropland. Between predictors are location means. Response units are μmol m^{-2}; predictor units are °C, m^3 m^{-3}, m, kg km^{-2} yr^{-1} for inventories, and a dimensionless cropland fraction.

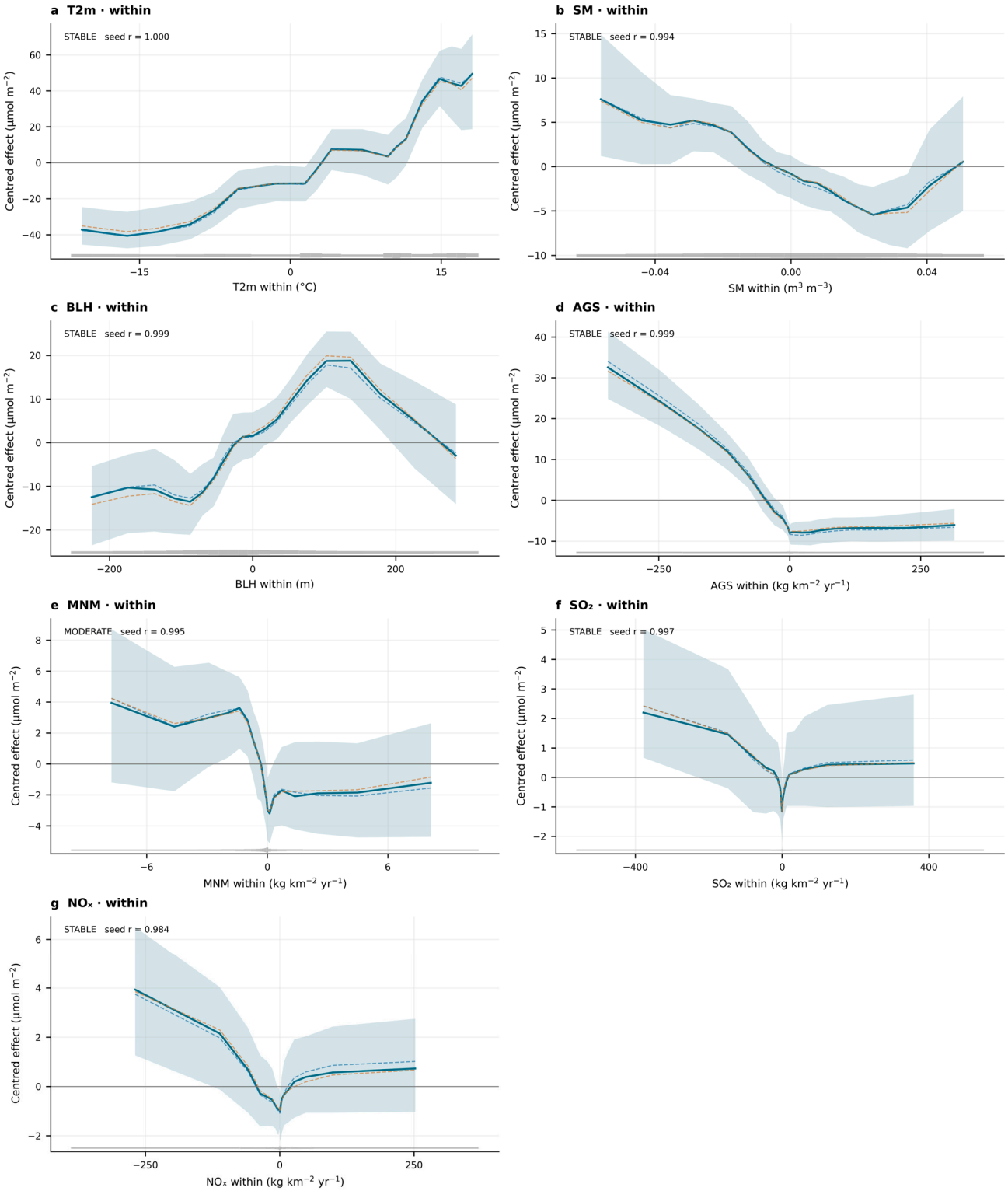


Figure S10. All seven within-location dynamic-driver ALE curves, with forest median, approximate 95% forest-response band, seed means and density strips as in Fig. S9. EDGAR emission departures represent annual rather than monthly variability. Cropland has no within component. Effect estimates use 2008–2022. Panels (a–g) show T2m, SM, BLH, AGS, MNM, SO_2 and NO_x departures from location means. Response and predictor units follow Fig. S9.

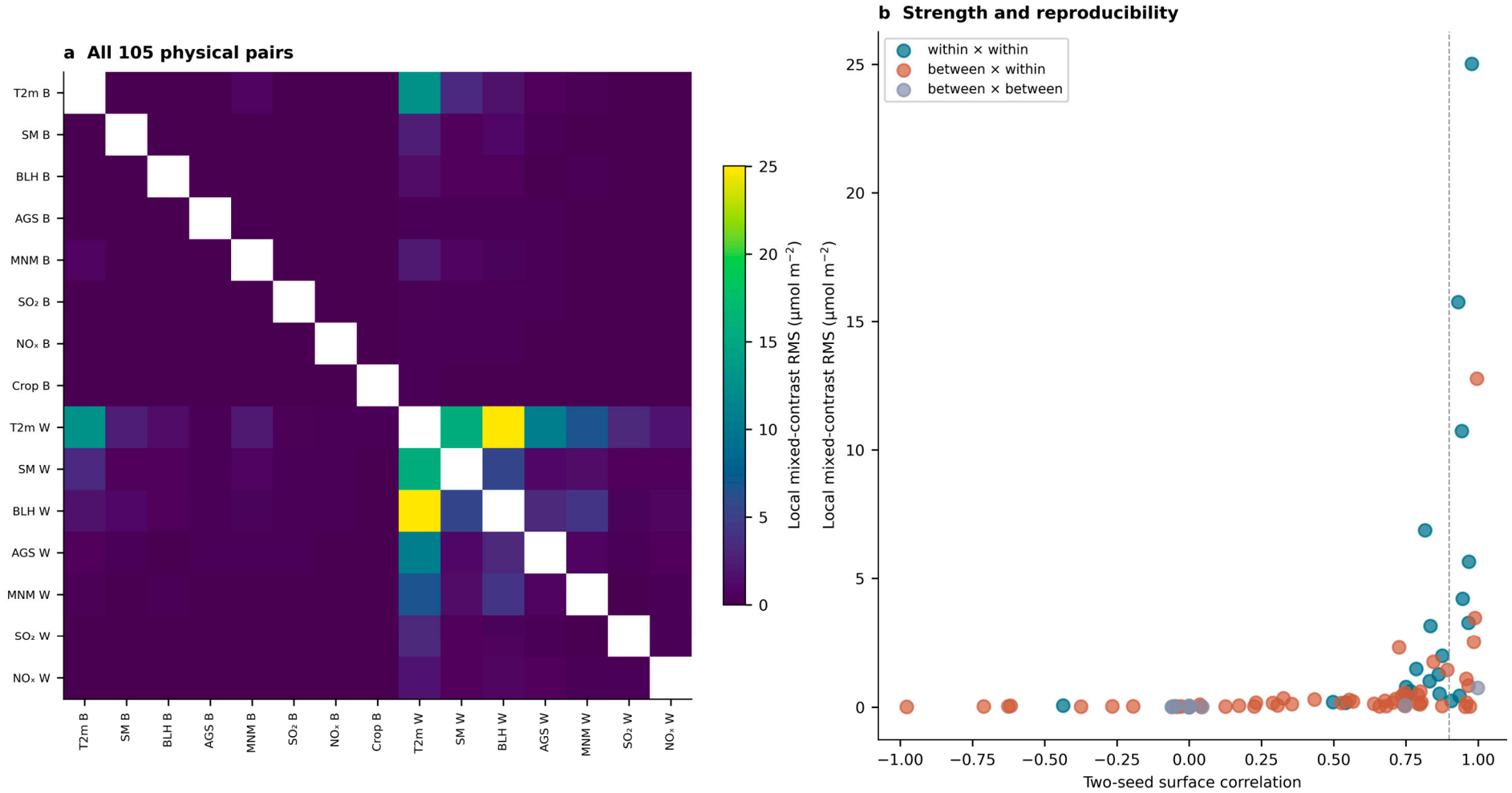


Figure S11. Complete screening of all 105 physical-component pairs. (a) Frequency-weighted local mixed-contrast RMS matrix. B and W denote between and within components. (b) RMS versus two-seed surface correlation, grouped by interaction type; symbol size reflects the fraction of central-range data supported by eligible cells. The dashed line marks r = 0.90. The full screening results, including unsupported or unstable pairs, are retained in Table S14. Effect estimates use 2008–2022. RMS units are μmol m^{-2}, while surface correlation and supported-data fractions are dimensionless. Between predictors are location means and within predictors are departures from those means.

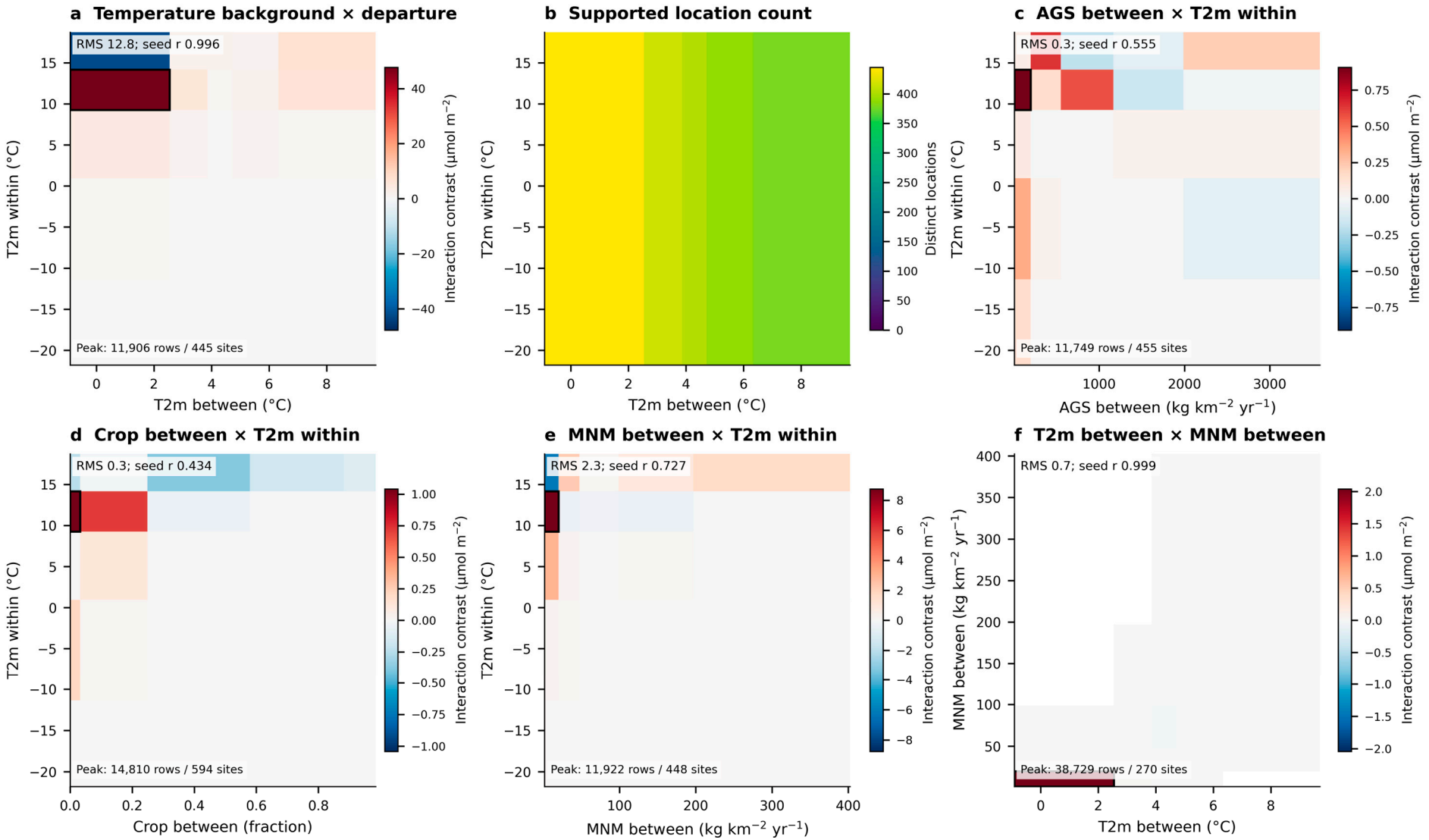


Figure S12. Supplementary interaction evidence. (a) Temperature between × temperature within local mixed contrast and (b) its distinct-location support. (c–e) Agricultural background × temperature departure contrasts for AGS, cropland and MNM, with seed reproducibility shown; these surfaces are screening diagnostics rather than principal mechanism claims. (f) Temperature between × MNM between contrast as spatial-background evidence. Colour definitions and support requirements follow Fig. 5. Effect estimates use 2008–2022. Contrasts are in μmol m⁻² and support in distinct locations. Temperature is in °C, annual emission density in kg km⁻² yr⁻¹ and cropland in fractions. Between predictors are location means; within predictors are departures. White masked cells have insufficient support.

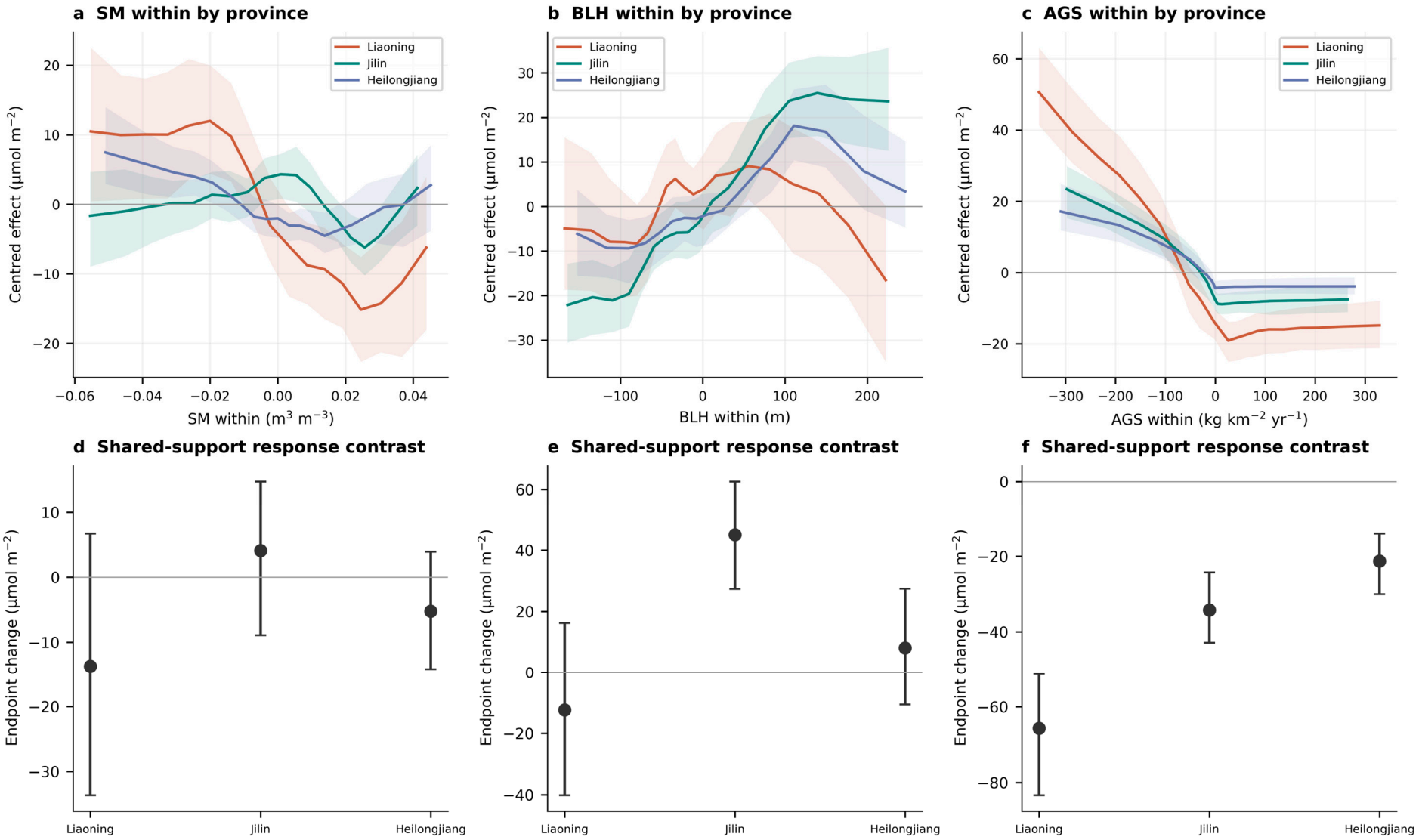


Figure S13. Province heterogeneity for additional drivers from the same full UST-BART model. (a–c) Soil-moisture, BLH and AGS within ALE curves restricted to shared provincial P5–P95 support; lines are forest medians and shading approximate 95% forest-response bands. (d–f) Forest-mean endpoint contrasts with approximate 95% forest-response bands over those shared ranges. Each province curve is centred within its reference distribution. AGS reflects annual variability. Effect estimates use 2008–2022. Within predictors are departures from location means. Response and endpoint-contrast units are μmol m^{-2}; SM, BLH and AGS units are m^3 m^{-3}, m and kg km^{-2} yr^{-1}, respectively.

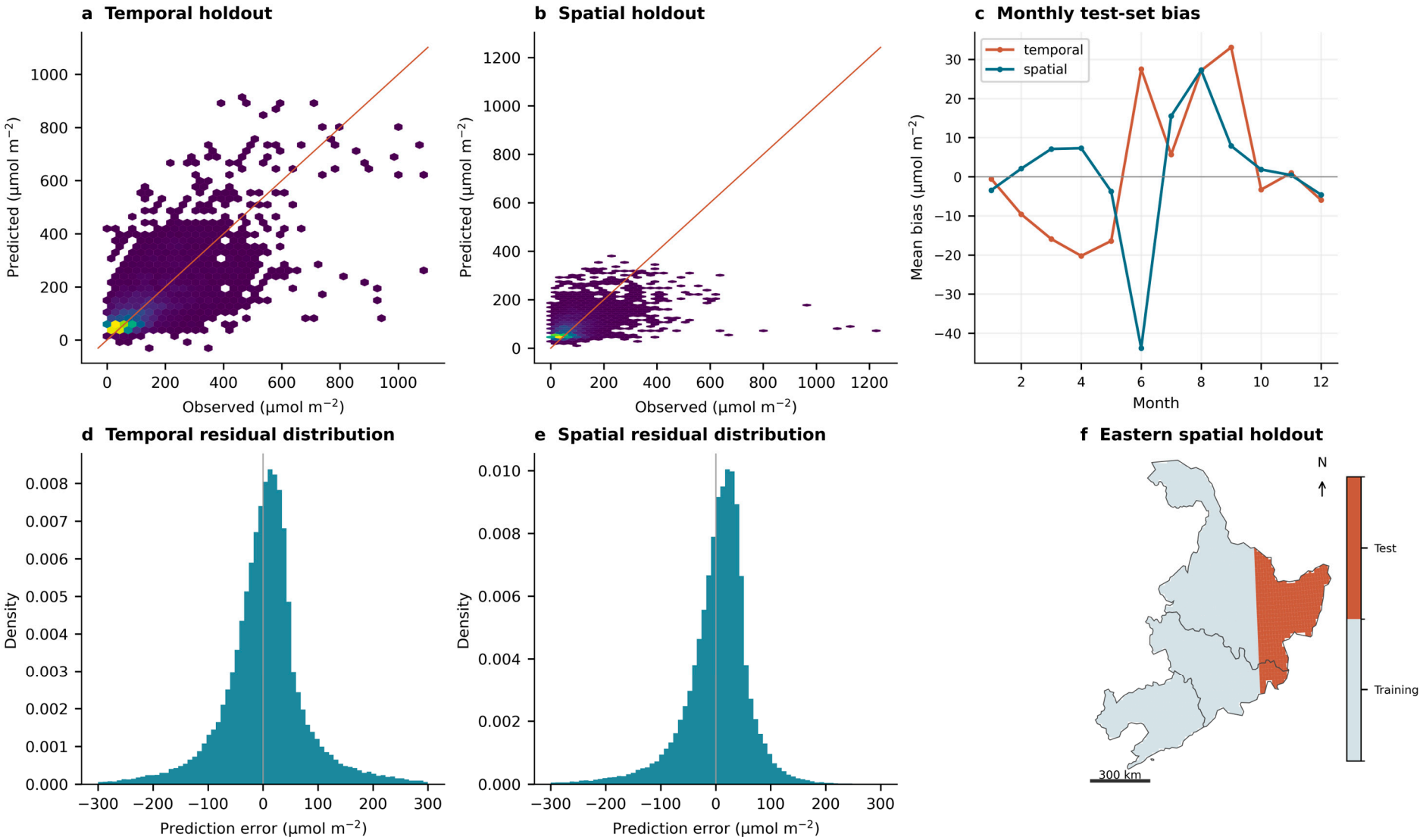


Figure S14. Independent validation of UST-BART. (a, b) Observed versus predicted NH_3 for deterministic evenly spaced 6,000-row subsets of the temporal and spatial tests, shown as hexagonal counts with the identity line. (c) Monthly biases from all test rows. (d, e) Prediction-error distributions from all test rows, displayed from −300 to +300 μmol m^{-2}. (f) Continuous eastern spatial holdout (longitude ≥129.5°E). Temporal training was 2008–2018 and testing 2019–2022. Metrics in Table 2A and Table S16 use all test rows. Projection follows Fig. 2.

Supplementary tables

Table S1A. Overpass and low-support sensitivity

Region	overpass	support filter	TS / decade	early amplitude	late amplitude	amplitude percent increase
NE3	AM	No	4.79e-05	0.000128	0.000281	119.78
NE3	AM	Yes	4.77e-05	0.000128	0.000281	120.24
NE3	AMPM	No	4.52e-05	0.000118	0.000259	119.68
NE3	AMPM	Yes	4.53e-05	0.000118	0.000259	119.46
Liaoning	AM	No	0.000101	0.000305	0.000496	62.52
Liaoning	AM	Yes	0.0001	0.000306	0.000497	62.56
Liaoning	AMPM	No	9.83e-05	0.000273	0.000447	63.56
Liaoning	AMPM	Yes	9.82e-05	0.000273	0.000447	63.61
Jilin	AM	No	5.89e-05	0.000165	0.000308	86.34
Jilin	AM	Yes	5.88e-05	0.000166	0.00031	86.70
Jilin	AMPM	No	5.58e-05	0.000157	0.00029	85.08
Jilin	AMPM	Yes	5.6e-05	0.000157	0.00029	84.84
Heilongjiang	AM	No	2.44e-05	9.1e-05	0.000198	117.76
Heilongjiang	AM	Yes	2.47e-05	9.06e-05	0.000198	119.07
Heilongjiang	AMPM	No	2.16e-05	8.62e-05	0.000184	113.95
Heilongjiang	AMPM	Yes	2.17e-05	8.6e-05	0.000184	113.99

Slopes: mol m^{-2} $decade^{-1}$; amplitudes: mol m^{-2}. Support_filter true requires producer nobs ≥0.25. Same spatial weights and equal-month annual means, 2008–2024.

Table S1B. Negative retrieval prevalence

Region	overpass	support filter	negative area time fraction	Negative N	finite records
NE3	AM	No	0.156	72,422	453,386
NE3	AM	Yes	0.149	66,918	440,790
NE3	AMPM	No	0.127	60,672	464,225
NE3	AMPM	Yes	0.126	60,116	463,036
Liaoning	AM	No	0.091	7,786	84,389
Liaoning	AM	Yes	0.089	7,583	83,929
Liaoning	AMPM	No	0.053	4,614	84,653
Liaoning	AMPM	Yes	0.053	4,607	84,632
Jilin	AM	No	0.140	16,377	117,428
Jilin	AM	Yes	0.133	15,298	114,832
Jilin	AMPM	No	0.110	13,121	119,244
Jilin	AMPM	Yes	0.109	12,999	118,961
Heilongjiang	AM	No	0.186	50,943	270,698
Heilongjiang	AM	Yes	0.176	46,479	260,630
Heilongjiang	AMPM	No	0.159	45,236	279,860
Heilongjiang	AMPM	Yes	0.157	44,753	278,860

Negative fractions use administrative area × month weights. Counts are finite records overlapping each region. nobs is fractional, not an integer sample count.

Table S2. Data coverage and preprocessing

Variable	Year	Period	Potential N	Finite/valid N	Negative N	Unit
nh3	2008	descriptive	27,336	27,330	3,176	mol m^{-2}
nh3	2009	descriptive	27,336	27,327	4,157	mol m^{-2}
nh3	2010	descriptive	27,336	27,272	4,430	mol m^{-2}
nh3	2011	descriptive	27,336	27,308	3,847	mol m^{-2}
nh3	2012	descriptive	27,336	27,303	4,207	mol m^{-2}
nh3	2013	descriptive	27,336	27,324	4,718	mol m^{-2}
nh3	2014	descriptive	27,336	27,314	3,670	mol m^{-2}
nh3	2015	descriptive	27,336	27,329	3,425	mol m^{-2}
nh3	2016	descriptive	27,336	27,295	3,777	mol m^{-2}
nh3	2017	descriptive	27,336	27,314	3,538	mol m^{-2}
nh3	2018	descriptive	27,336	27,273	3,077	mol m^{-2}
nh3	2019	descriptive	27,336	27,329	3,098	mol m^{-2}
nh3	2020	descriptive	27,336	27,318	3,490	mol m^{-2}
nh3	2021	descriptive	27,336	27,301	3,102	mol m^{-2}
nh3	2022	descriptive	27,336	27,309	3,117	mol m^{-2}
nh3	2023	descriptive	27,336	27,293	3,028	mol m^{-2}
nh3	2024	descriptive	27,336	27,286	2,815	mol m^{-2}
nh3_nobs	2008	descriptive	27,336	27,336	0	1 (fractional)
nh3_nobs	2009	descriptive	27,336	27,336	0	1 (fractional)
nh3_nobs	2010	descriptive	27,336	27,336	0	1 (fractional)
nh3_nobs	2011	descriptive	27,336	27,336	0	1 (fractional)
nh3_nobs	2012	descriptive	27,336	27,336	0	1 (fractional)
nh3_nobs	2013	descriptive	27,336	27,336	0	1 (fractional)
nh3_nobs	2014	descriptive	27,336	27,336	0	1 (fractional)
nh3_nobs	2015	descriptive	27,336	27,336	0	1 (fractional)
nh3_nobs	2016	descriptive	27,336	27,336	0	1 (fractional)
nh3_nobs	2017	descriptive	27,336	27,336	0	1 (fractional)
nh3_nobs	2018	descriptive	27,336	27,336	0	1 (fractional)
nh3_nobs	2019	descriptive	27,336	27,336	0	1 (fractional)
nh3_nobs	2020	descriptive	27,336	27,336	0	1 (fractional)
nh3_nobs	2021	descriptive	27,336	27,336	0	1 (fractional)
nh3_nobs	2022	descriptive	27,336	27,336	0	1 (fractional)
nh3_nobs	2023	descriptive	27,336	27,336	0	1 (fractional)
nh3_nobs	2024	descriptive	27,336	27,336	0	1 (fractional)
nh3_unc_random	2008	descriptive	27,336	27,330	0	mol m^{-2}
nh3_unc_random	2009	descriptive	27,336	27,327	0	mol m^{-2}
nh3_unc_random	2010	descriptive	27,336	27,272	0	mol m^{-2}
nh3_unc_random	2011	descriptive	27,336	27,308	0	mol m^{-2}
nh3_unc_random	2012	descriptive	27,336	27,303	0	mol m^{-2}
nh3_unc_random	2013	descriptive	27,336	27,324	0	mol m^{-2}

Variable	Year	Period	Potential N	Finite/valid N	Negative N	Unit
nh3_unc_random	2014	descriptive	27,336	27,314	0	mol m⁻²
nh3_unc_random	2015	descriptive	27,336	27,329	0	mol m⁻²
nh3_unc_random	2016	descriptive	27,336	27,295	0	mol m⁻²
nh3_unc_random	2017	descriptive	27,336	27,314	0	mol m⁻²
nh3_unc_random	2018	descriptive	27,336	27,273	0	mol m⁻²
nh3_unc_random	2019	descriptive	27,336	27,329	0	mol m⁻²
nh3_unc_random	2020	descriptive	27,336	27,318	0	mol m⁻²
nh3_unc_random	2021	descriptive	27,336	27,301	0	mol m⁻²
nh3_unc_random	2022	descriptive	27,336	27,309	0	mol m⁻²
nh3_unc_random	2023	descriptive	27,336	27,293	0	mol m⁻²
nh3_unc_random	2024	descriptive	27,336	27,286	0	mol m⁻²
nh3_unc_systematic	2008	descriptive	27,336	27,330	0	mol m⁻²
nh3_unc_systematic	2009	descriptive	27,336	27,327	0	mol m⁻²
nh3_unc_systematic	2010	descriptive	27,336	27,272	0	mol m⁻²
nh3_unc_systematic	2011	descriptive	27,336	27,308	0	mol m⁻²
nh3_unc_systematic	2012	descriptive	27,336	27,303	0	mol m⁻²
nh3_unc_systematic	2013	descriptive	27,336	27,324	0	mol m⁻²
nh3_unc_systematic	2014	descriptive	27,336	27,314	0	mol m⁻²
nh3_unc_systematic	2015	descriptive	27,336	27,329	0	mol m⁻²
nh3_unc_systematic	2016	descriptive	27,336	27,295	0	mol m⁻²
nh3_unc_systematic	2017	descriptive	27,336	27,314	0	mol m⁻²
nh3_unc_systematic	2018	descriptive	27,336	27,273	0	mol m⁻²
nh3_unc_systematic	2019	descriptive	27,336	27,329	0	mol m⁻²
nh3_unc_systematic	2020	descriptive	27,336	27,318	0	mol m⁻²
nh3_unc_systematic	2021	descriptive	27,336	27,301	0	mol m⁻²
nh3_unc_systematic	2022	descriptive	27,336	27,309	0	mol m⁻²
nh3_unc_systematic	2023	descriptive	27,336	27,293	0	mol m⁻²
nh3_unc_systematic	2024	descriptive	27,336	27,286	0	mol m⁻²
T2m	2008	descriptive	27,336	27,336	9,507	°C
T2m	2009	descriptive	27,336	27,336	11,152	°C
T2m	2010	descriptive	27,336	27,336	11,380	°C
T2m	2011	descriptive	27,336	27,336	10,806	°C
T2m	2012	descriptive	27,336	27,336	11,240	°C
T2m	2013	descriptive	27,336	27,336	11,183	°C
T2m	2014	descriptive	27,336	27,336	10,504	°C
T2m	2015	descriptive	27,336	27,336	10,889	°C
T2m	2016	descriptive	27,336	27,336	10,949	°C
T2m	2017	descriptive	27,336	27,336	10,842	°C
T2m	2018	descriptive	27,336	27,336	10,620	°C
T2m	2019	descriptive	27,336	27,336	10,328	°C
T2m	2020	descriptive	27,336	27,336	10,497	°C

Variable	Year	Period	Potential N	Finite/valid N	Negative N	Unit
T2m	2021	descriptive	27,336	27,336	10,305	°C
T2m	2022	descriptive	27,336	27,336	10,644	°C
T2m	2023	descriptive	27,336	27,336	9,792	°C
T2m	2024	descriptive	27,336	27,336	10,570	°C
SM	2008	descriptive	27,336	27,336	0	$m^3\ m^{-3}$
SM	2009	descriptive	27,336	27,336	0	$m^3\ m^{-3}$
SM	2010	descriptive	27,336	27,336	0	$m^3\ m^{-3}$
SM	2011	descriptive	27,336	27,336	0	$m^3\ m^{-3}$
SM	2012	descriptive	27,336	27,336	0	$m^3\ m^{-3}$
SM	2013	descriptive	27,336	27,336	0	$m^3\ m^{-3}$
SM	2014	descriptive	27,336	27,336	0	$m^3\ m^{-3}$
SM	2015	descriptive	27,336	27,336	0	$m^3\ m^{-3}$
SM	2016	descriptive	27,336	27,336	0	$m^3\ m^{-3}$
SM	2017	descriptive	27,336	27,336	0	$m^3\ m^{-3}$
SM	2018	descriptive	27,336	27,336	0	$m^3\ m^{-3}$
SM	2019	descriptive	27,336	27,336	0	$m^3\ m^{-3}$
SM	2020	descriptive	27,336	27,336	0	$m^3\ m^{-3}$
SM	2021	descriptive	27,336	27,336	0	$m^3\ m^{-3}$
SM	2022	descriptive	27,336	27,336	0	$m^3\ m^{-3}$
SM	2023	descriptive	27,336	27,336	0	$m^3\ m^{-3}$
SM	2024	descriptive	27,336	27,336	0	$m^3\ m^{-3}$
BLH	2008	descriptive	27,336	27,336	0	m
BLH	2009	descriptive	27,336	27,336	0	m
BLH	2010	descriptive	27,336	27,336	0	m
BLH	2011	descriptive	27,336	27,336	0	m
BLH	2012	descriptive	27,336	27,336	0	m
BLH	2013	descriptive	27,336	27,336	0	m
BLH	2014	descriptive	27,336	27,336	0	m
BLH	2015	descriptive	27,336	27,336	0	m
BLH	2016	descriptive	27,336	27,336	0	m
BLH	2017	descriptive	27,336	27,336	0	m
BLH	2018	descriptive	27,336	27,336	0	m
BLH	2019	descriptive	27,336	27,336	0	m
BLH	2020	descriptive	27,336	27,336	0	m
BLH	2021	descriptive	27,336	27,336	0	m
BLH	2022	descriptive	27,336	27,336	0	m
BLH	2023	descriptive	27,336	27,336	0	m
BLH	2024	descriptive	27,336	27,336	0	m
nh3 mechanism	2008	2008–2022	410,040	354,539	54,829	$mol\ m^{-2}$

Descriptive analyses retain negative retrievals. Mechanism rows require nonnegative response and all eight physical predictors. Negative temperature counts are descriptive, not exclusions. Units refer to the harmonized/source fields before the model response conversion to $\mu mol\ m^{-2}$. The complete coverage table preserves each variable/year support.

Table S3A. Regional/provincial trends and sensitivity

Region	Variant	TS / decade	TS lower	TS upper	MK p	HAC(1) p	HAC(2) p
NE3	nh3	4.52	3.12	5.70	9.1e-05	1.25e-06	1.27e-06
NE3	nobs_weighted_sensitivity	4.02	2.28	5.33	0.000246	1.55e-05	1.83e-05
NE3	area_mean_cell_annual	4.53	3.12	5.71	9.1e-05	1.25e-06	1.28e-06
Liaoning	nh3	9.83	7.05	12.09	7.12e-06	6.78e-07	5.14e-07
Liaoning	nobs_weighted_sensitivity	8.53	6.68	11.24	3.24e-06	3.31e-06	2.52e-06
Liaoning	area_mean_cell_annual	9.83	7.05	12.09	7.12e-06	6.78e-07	5.14e-07
Jilin	nh3	5.58	3.57	6.76	0.000246	3.13e-06	3.01e-06
Jilin	nobs_weighted_sensitivity	4.72	3.25	6.16	0.000178	5.22e-06	6.08e-06
Jilin	area_mean_cell_annual	5.59	3.57	6.76	0.000246	3.15e-06	3.02e-06
Heilongjiang	nh3	2.16	1.19	3.33	0.002	1.88e-05	1.31e-05
Heilongjiang	nobs_weighted_sensitivity	1.55	0.554	3.04	0.009	0.001	0.001
Heilongjiang	area_mean_cell_annual	2.16	1.19	3.33	0.002	1.88e-05	1.31e-05

Slope and confidence bounds: 10^{-5} mol m^{-2} decade^{-1}. Ordinary MK p-values are not autocorrelation-corrected; HAC is the regional/provincial sensitivity. Variants use equal-month means, observation-support weighting or area means of cell-annual values.

Table S3B. Spatial distribution of trends and period changes

Region	P25	median	P75	Positive area (%)	Increasing FDR area (%)	Late − Early
NE3	1.87	3.98	6.29	93.63	71.20	0.502
Liaoning	7.61	9.67	11.61	100.00	100.00	1.11
Jilin	4.22	5.40	6.52	100.00	96.85	0.601
Heilongjiang	0.821	2.31	3.73	88.79	50.66	0.259

Cell slope quantiles: 10^{-5} mol m^{-2} decade^{-1}; area shares: %. Early–Late changes: 10^{-4} mol m^{-2}. Fractions use represented administrative overlap area.

Table S4A. Mechanism-period exclusions by province, month and year

Group	Level	N	negative	Negative fraction	Other excluded	Other fraction	Model valid N
province	Heilongjiang	241,200	39,803	0.165	604	0.003	200,793
province	Jilin	96,480	10,873	0.113	61	0.000632	85,546
province	Liaoning	72,360	4,153	0.057	7	9.67e-05	68,200
month	1	34,170	9,625	0.282	166	0.005	24,379
month	2	34,170	8,398	0.246	88	0.003	25,684
month	3	34,170	4,051	0.119	25	0.000732	30,094
month	4	34,170	1,885	0.055	25	0.000732	32,260
month	5	34,170	1,470	0.043	23	0.000673	32,677
month	6	34,170	1,806	0.053	28	0.000819	32,336
month	7	34,170	2,029	0.059	23	0.000673	32,118
month	8	34,170	3,705	0.108	27	0.00079	30,438

Group	Level	N	negative	Negative fraction	Other excluded	Other fraction	Model valid N
month	9	34,170	2,464	0.072	28	0.000819	31,678
month	10	34,170	2,506	0.073	29	0.000849	31,635
month	11	34,170	6,901	0.202	30	0.000878	27,239
month	12	34,170	9,989	0.292	180	0.005	24,001
year	2008	27,336	3,176	0.116	29	0.001	24,131
year	2009	27,336	4,157	0.152	26	0.000951	23,153
year	2010	27,336	4,430	0.162	85	0.003	22,821
year	2011	27,336	3,847	0.141	48	0.002	23,441
year	2012	27,336	4,207	0.154	46	0.002	23,083
year	2013	27,336	4,718	0.173	26	0.000951	22,592
year	2014	27,336	3,670	0.134	44	0.002	23,622
year	2015	27,336	3,425	0.125	26	0.000951	23,885
year	2016	27,336	3,777	0.138	61	0.002	23,498
year	2017	27,336	3,538	0.129	43	0.002	23,755
year	2018	27,336	3,077	0.113	80	0.003	24,179
year	2019	27,336	3,098	0.113	25	0.000915	24,213
year	2020	27,336	3,490	0.128	34	0.001	23,812
year	2021	27,336	3,102	0.113	52	0.002	24,182
year	2022	27,336	3,117	0.114	47	0.002	24,172

Fractions are dimensionless. Other exclusions are mutually exclusive of negative-response rows. Total: 410,040 candidates, 54,829 negative responses, 672 other exclusions, 354,539 valid.

Table S4B. Response distributions before and after selection

Region	sample	N	Negative fraction	mean	SD	median	P25
NE3	all finite	409,646	0.134	83.39	108.85	56.97	19.95
NE3	model valid	354,539	0	100.61	106.43	68.53	34.61
Liaoning	all finite	72,353	0.057	148.15	154.16	103.53	48.30
Liaoning	model valid	68,200	0	158.68	152.46	111.70	57.14
Jilin	all finite	96,419	0.113	90.91	103.46	67.03	26.62
Jilin	model valid	85,546	0	106.35	99.07	77.49	40.11
Heilongjiang	all finite	240,874	0.165	60.92	83.29	44.84	12.83
Heilongjiang	model valid	200,793	0	78.44	79.21	56.46	28.69

Unweighted cell-month summaries in μmol m^{-2}, 2008–2022. Province labels use the largest overlap; Fig. S4 instead uses fractional administrative area weights. Negative retrievals can arise from noise/sensitivity and are retained in descriptive analysis.

Table S4B. Response distributions before and after selection (continued measures)

Region	sample	P75	units
NE3	all finite	114.11	micromol m-2
NE3	model valid	126.91	micromol m-2
Liaoning	all finite	198.59	micromol m-2
Liaoning	model valid	207.31	micromol m-2
Jilin	all finite	127.62	micromol m-2
Jilin	model valid	138.30	micromol m-2
Heilongjiang	all finite	88.48	micromol m-2
Heilongjiang	model valid	100.12	micromol m-2

Unweighted cell-month summaries in μmol m^{-2}, 2008–2022. Province labels use the largest overlap; Fig. S4 instead uses fractional administrative area weights. Negative retrievals can arise from noise/sensitivity and are retained in descriptive analysis.

Table S4C. Locations omitted entirely from mechanism analysis

cell id	lon	lat	Province	N	negative	Other excluded	Crop missing N
NE3_R675_C1561	132.30	45.10	Heilongjiang	180	36	144	180
NE3_R675_C1562	132.50	45.10	Heilongjiang	180	46	134	180

Both cells have missing cropland for all 180 months. Negative and other exclusions sum to 180 separately at each location.

Table S5. Driver distributions on valid model support

Variable	units	Time support	N	mean	SD	median	P25
T2m	deg C	cell-month 2008–2022	354,539	5.78	13.88	8.05	-5.41
SM	m3 m-3	cell-month 2008–2022	354,539	0.327	0.050	0.338	0.302
BLH	m	cell-month 2008–2022	354,539	549.78	168.14	528.95	446.94
AGS	kg km-2 yr-1	cell-year 2008–2022	34,140	1117.27	1155.82	696.67	183.68
MNM	kg km-2 yr-1	cell-year 2008–2022	34,140	116.92	138.67	60.46	18.91
SO_2	kg km-2 yr-1	cell-year 2008–2022	34,140	2444.94	1.44e+04	242.63	43.11
NO_x	kg km-2 yr-1	cell-year 2008–2022	34,140	2176.14	9073.46	431.72	97.36
cropland_fraction	1	cell, 2020 static	2,276	0.426	0.380	0.349	0.028

Meteorology: cell-months; annual inventories: each cell-year counted once; 2020 cropland: once per location. Source values are not demeaned here. Full tails are retained in Fig. S5; min/max and P5/P95 remain in the accompanying CSV.

Table S5. Driver distributions on valid model support (continued measures)

Variable	units	P75	IQR
T2m	deg C	17.99	23.39
SM	m3 m-3	0.363	0.061
BLH	m	645.55	198.61
AGS	kg km-2 yr-1	1761.35	1577.67
MNM	kg km-2 yr-1	164.42	145.51
SO_2	kg km-2 yr-1	786.83	743.72
NO_x	kg km-2 yr-1	1159.70	1062.35
cropland_fraction	1	0.836	0.808

Meteorology: cell-months; annual inventories: each cell-year counted once; 2020 cropland: once per location. Source values are not demeaned here. Full tails are retained in Fig. S5; min/max and P5/P95 remain in the accompanying CSV.

Table S6. Autocorrelation-aware trend uncertainty and field significance, 2008–2024

Table S6A. Regional and provincial Theil–Sen trend uncertainty from temporal block bootstrap

Region	Block (years)	Theil–Sen slope	95% block-bootstrap CI	Bootstrap p
NE3	2	45.24	[33.65, 55.82]	0.0005
NE3	3	45.24	[33.41, 55.02]	0.0005
Liaoning	2	98.30	[75.73, 118.69]	0.0005
Liaoning	3	98.30	[77.10, 117.93]	0.0005
Jilin	2	55.83	[41.17, 68.54]	0.0005
Jilin	3	55.83	[39.80, 69.10]	0.0005
Heilongjiang	2	21.63	[13.72, 28.94]	0.0005
Heilongjiang	3	21.63	[12.81, 28.86]	0.0005

Notes. Slopes and confidence intervals are in μmol m^{-2} $decade^{-1}$. Each region has 17 annual observations. Confidence intervals use circular moving-block resampling of centred, Theil–Sen-detrended annual residuals (1,999 replicates); two- and three-year blocks are reported separately. Bootstrap p-values have a minimum reporting resolution of 0.0005.

Table S6B. Spatial field significance of the positive NH_3 trend area

Block (years)	Positive area (%)	Null P95 area (%)	Field one-sided p	Regional null two-sided p
2	93.63	74.01	0.0005	0.0005
3	93.63	75.38	0.0005	0.0005

Notes. Positive area is the administrative-overlap-area fraction of 2,278 cells with a positive annual Theil–Sen slope (observed: 93.63%). The no-trend reference distribution was constructed by detrending and centring each cell's annual series, then resampling common circular year-block indices across all cells (1,999 replicates). Null P95 is the 95th percentile of positive-area fractions under this reference distribution. Regional null p tests the trend in the area-weighted annual cell field (45.29 μmol m^{-2} $decade^{-1}$), which differs slightly from the main equal-month regional trend (45.24 μmol m^{-2} $decade^{-1}$) because aggregation order differs. Field-level p-values do not replace the original unadjusted cell-level Mann–Kendall/BH–FDR classifications.

Table S7. Seasonality definitions and changes

Region	Definition	early	late	late minus early	percent change	amplitude increased area fraction
Heilongjiang	JJA_minus_DJF	0.533	1.31	0.780	146.37	0.960
Heilongjiang	harmonic_peak_to_trough	0.610	1.41	0.800	131.24	0.960
Heilongjiang	max_minus_min	0.862	1.84	0.982	113.95	0.960
Jilin	JJA_minus_DJF	1.04	2.21	1.18	113.15	0.973
Jilin	harmonic_peak_to_trough	1.16	2.39	1.23	105.62	0.973
Jilin	max_minus_min	1.57	2.90	1.33	85.08	0.973
Liaoning	JJA_minus_DJF	1.75	3.42	1.67	95.64	0.982
Liaoning	harmonic_peak_to_trough	1.93	3.63	1.70	88.19	0.982
Liaoning	max_minus_min	2.73	4.47	1.74	63.56	0.982
NE3	JJA_minus_DJF	0.884	1.93	1.04	118.02	0.967
NE3	harmonic_peak_to_trough	0.992	2.06	1.07	108.00	0.967
NE3	max_minus_min	1.18	2.59	1.41	119.68	0.967

Early 2008–2012 and Late 2019–2024. Early/late amplitude and difference: 10^{-4} mol m^{-2}. Percent increase uses unrounded amplitudes. Amplitude-increased area fraction is dimensionless.

Table S8. Instrument-transition and seasonal-amplification sensitivity analyses

Contemporaneous paired instruments, transition-year bridging, instrument-specific trends, change-point analyses and retrieval characteristics were evaluated for 2008–2024. The primary MERGED record was retained throughout the main analysis.

Table S8A. Contemporaneous instrument comparisons and transition-year bridging

Region	Transition	Overlap Δmean	Overlap Δampl.	Annual Δ merged / same	Amplitude Δ merged / same
NE3	2014: A→B	+5.17	+18.11	+32.52 / +27.34	+121.77 / +103.71
NE3	2020: B→C	-6.85	-36.57	+0.47 / +7.35	-35.28 / +1.20
Liaoning	2014: A→B	+10.95	+50.66	+55.55 / +44.60	+210.39 / +159.73
Liaoning	2020: B→C	-9.48	-53.25	+10.94 / +20.41	-69.90 / -16.65
Jilin	2014: A→B	+6.12	+43.41	+37.28 / +31.14	+172.65 / +129.50
Jilin	2020: B→C	-10.62	-70.49	+5.56 / +16.23	-32.33 / +37.82
Heilongjiang	2014: A→B	+2.86	+12.75	+22.86 / +20.00	+87.79 / +74.96
Heilongjiang	2020: B→C	-4.36	-14.87	-5.17 / -0.80	-22.34 / -7.47

Notes. All differences in μmol m^{-2}. Overlap columns compare twelve contemporaneous monthly Level-3 fields in 2014 (A/B) or 2020 (B/C) on common finite cells with identical area weights. The bridging columns compare 2013–2014 using Metop-A, or 2019–2020 using Metop-B, on common three-field support. Overlap and bridge supports may differ slightly; contemporaneous offsets are not pure calibration estimates.

Table S8B. Instrument-period trends and seasonal-amplitude changes

Region	Instrument (years)	TS slope	2-year block 95% CI	Independent-year TS CI	Amplitude early → late	Change % [95% CI]
NE3	A (2008–2013)	-7.06	[-14.48, 0.63]	[-38.18, 37.84]	108.65 → 129.32	+19.02 [-14.34, 74.44]
NE3	B (2014–2019)	+3.57	[-21.07, 13.70]	[-36.03, 98.11]	252.47 → 237.79	-5.82 [-16.78, 13.96]
NE3	C (2020–2024)	+121.05	[72.87, 170.66]	[-96.58, 356.83]	226.09 → 334.87	+48.12 [20.98, 87.03]
Liaoning	A (2008–2013)	-3.97	[-53.22, 32.97]	[-112.47, 140.50]	266.65 → 263.78	-1.08 [-36.80, 71.10]
Liaoning	B (2014–2019)	+42.40	[25.78, 75.57]	[9.23, 311.67]	438.03 → 504.39	+15.15 [-5.69, 36.27]
Liaoning	C (2020–2024)	+218.87	[117.67, 306.58]	[-118.07, 701.30]	349.51 → 644.19	+84.31 [41.94, 120.71]
Jilin	A (2008–2013)	-5.25	[-12.42, 5.55]	[-48.43, 41.44]	133.58 → 170.51	+27.65 [-13.02, 90.10]
Jilin	B (2014–2019)	+0.49	[-19.67, 20.64]	[-87.60, 105.38]	300.97 → 274.37	-8.84 [-23.62, 10.52]
Jilin	C (2020–2024)	+143.36	[86.92, 186.15]	[-26.52, 421.98]	246.27 → 424.11	+72.21 [52.02, 93.46]
Heilongjiang	A (2008–2013)	-15.07	[-27.56, 4.73]	[-52.52, 26.91]	82.90 → 97.92	+18.12 [-28.27, 68.27]
Heilongjiang	B (2014–2019)	-6.03	[-24.56, 7.74]	[-61.63, 44.90]	170.34 → 148.50	-12.82 [-26.53, -0.84]
Heilongjiang	C (2020–2024)	+53.77	[3.29, 103.04]	[-198.41, 269.91]	191.58 → 216.56	+13.04 [-17.27, 100.33]

Notes. Slopes and intervals in μmol m^{-2} $decade^{-1}$; amplitudes in μmol m^{-2}. Block confidence intervals use two-year circular moving blocks; independent-year Theil–Sen intervals are reported separately for the five- or six-year periods. Amplitude comparisons are 2008–2010 vs. 2011–2013 (A), 2014–2016 vs. 2017–2019 (B), and 2020–2021 vs. 2023–2024 (C). Resampling uses complete annual 12-month vectors; 2022 enters the C trend but not its amplitude subperiod comparison.

Table S8C(a). Prespecified seasonally adjusted transition steps

Region	Year	Step (μmol m^{-2})	95% block interval	Month-specific step ΔBIC
NE3	2014	+15.17	[-5.39, 35.23]	+39.21
NE3	2020	+6.46	[-12.53, 25.54]	+45.26
Liaoning	2014	+13.60	[-28.15, 54.43]	+52.14
Liaoning	2020	+1.84	[-36.84, 38.42]	+39.43
Jilin	2014	+16.60	[-8.18, 41.10]	+47.06
Jilin	2020	+7.00	[-16.63, 30.50]	+48.62
Heilongjiang	2014	+15.09	[0.37, 30.26]	+40.58
Heilongjiang	2020	+7.72	[-6.39, 21.97]	+53.46

Notes. 204 monthly observations in 2008–2024. Step coefficients use month effects and temporal trends; 95% intervals use 12-month circular moving blocks (1,999 replicates). The month-specific ΔBIC comes from a separate model permitting month-specific trends. Positive ΔBIC does not favour the added step. Neither coefficient identifies instrument calibration changes on its own.

Table S8C(b). Unknown single-change-point screening

Region	Best candidate	Bootstrap break range	ΔBIC vs. no break
NE3	2011-03	2011-01 – 2021-10	+1.81
Liaoning	2011-03	2011-01 – 2021-10	+0.40
Jilin	2011-04	2011-01 – 2021-09	+2.01
Heilongjiang	2021-03	2011-04 – 2021-11	+2.02

Notes. The candidate break is the best of the scanned months; intervals use 12-month moving-block resampling (1,999 replicates). Positive ΔBIC means the best single-step model is not preferred to the no-step model.

Table S8D. Full-period sensitivity to monthly instrument-overlap offsets

Region	Scenario	TS slope	Early amplitude	Late amplitude	Increase (%)
NE3	Original MERGED	45.24	118.09	259.43	119.68
NE3	Offset scenario	46.27	118.09	258.38	118.79
Liaoning	Original MERGED	98.30	273.16	446.79	63.56
Liaoning	Offset scenario	92.11	273.16	465.42	70.38
Jilin	Original MERGED	55.83	156.75	290.12	85.08
Jilin	Offset scenario	53.14	156.75	281.04	79.29
Heilongjiang	Original MERGED	21.63	86.20	184.41	113.95
Heilongjiang	Offset scenario	23.07	86.20	180.32	109.20

Notes. Slopes in μmol m^{-2} $decade^{-1}$; amplitudes in μmol m^{-2}. Early = 2008–2012; Late = 2019–2024. The offset scenario treats month-specific A/B and B/C differences in the 2014/2020 overlaps as time-invariant platform offsets relative to A. It is a diagnostic sensitivity rather than calibrated replacement data; all original area weighting and temporal aggregation are retained.

Table S8E. Seasonal retrieval diagnostics related to winter NH_3 detection

Month	Finite N	Negative retrievals (%)	Low support (%)
January	38,557	28.00	1.17
February	38,648	24.00	0.52
June	38,723	5.28	0.04
July	38,722	5.35	0.04
December	38,504	29.23	1.16

Notes. NE3, 2008–2024. Negative fractions use finite retrievals. Low support means the fractional producer observation-support field is <0.25. Thermal contrast was not directly measured; its effect on IASI NH_3 retrieval sensitivity is discussed in the manuscript [13].

Table S9A. Hotspot persistence and redistribution

Definition	Percentile	Region	Persistent area	Early frequency	Late frequency	Early NE3 share	Late NE3 share
relative	80.00	NE3	0.105	0.200	0.200	1.00	1.00
relative	80.00	Liaoning	0.484	0.544	0.731	0.511	0.687
relative	80.00	Jilin	0.055	0.215	0.199	0.263	0.243
relative	80.00	Heilongjiang	0.002	0.079	0.025	0.226	0.070
relative	90.00	NE3	0.064	0.100	0.100	1.00	1.00
relative	90.00	Liaoning	0.341	0.382	0.503	0.718	0.947
relative	90.00	Jilin	4.05e-05	0.051	0.017	0.125	0.042
relative	90.00	Heilongjiang	0	0.028	0.002	0.157	0.011
fixed	90.00	NE3	0.030	0.030	0.255	1.00	1.00
fixed	90.00	Liaoning	0.161	0.148	0.770	0.872	0.642
fixed	90.00	Jilin	0	0.000388	0.302	0.003	0.243
fixed	90.00	Heilongjiang	0	0.004	0.064	0.125	0.114
relative	95.00	NE3	0.028	0.050	0.050	1.00	1.00
relative	95.00	Liaoning	0.148	0.229	0.264	0.862	0.997
relative	95.00	Jilin	0	0.005	0.000317	0.027	0.002
relative	95.00	Heilongjiang	0	0.010	0.00013	0.111	0.001

Fractions are dimensionless; persistence ≥0.8 means at least 14/17 years. Provincial frequencies use own-province area; hotspot shares use total NE3 hotspot area. Every cell has a finite annual value, based on 9–12 months. Strict percentile exceedance is used.

Table S9B. Centroid comparison and first-year influence

Definition	Percentile	Comparison	km	east km	north km
fixed	90.00	2008 to 2024	737.38	-618.07	-402.13
fixed	90.00	2009 to 2024	90.41	30.01	85.28
fixed	90.00	Early mean to Late mean	151.12	-130.59	-76.04
fixed	90.00	Early excluding 2008 to Late mean	24.95	2.79	24.79
relative	80.00	2008 to 2024	387.99	-244.65	-301.14
relative	80.00	2009 to 2024	59.13	-45.23	-38.07
relative	80.00	Early mean to Late mean	158.44	-98.77	-123.89
relative	80.00	Early excluding 2008 to Late mean	97.68	-58.87	-77.94
relative	90.00	2008 to 2024	477.38	-333.54	-341.53
relative	90.00	2009 to 2024	46.80	-33.44	-32.74
relative	90.00	Early mean to Late mean	163.49	-103.88	-126.25
relative	90.00	Early excluding 2008 to Late mean	81.24	-43.23	-68.79
relative	95.00	2008 to 2024	580.08	-429.87	-389.49
relative	95.00	2009 to 2024	51.27	-34.93	-37.53
relative	95.00	Early mean to Late mean	172.49	-113.07	-130.26
relative	95.00	Early excluding 2008 to Late mean	67.94	-31.49	-60.20

Distances are WGS84 geodesic km. Early/Late positions are arithmetic averages of annual centroid longitude/latitude; negative east/north components indicate west/south. This is a period-centroid sensitivity, not a migration model.

Table S10. Robust trends in hotspot-centroid coordinates and sensitivity to starting year and hotspot definition

Definition	Period	Coordinate	Theil–Sen slope (km yr^{-1})	95% bootstrap CI
Relative P90	2008–2024	East	−4.77	[−6.71, −2.53]
Relative P90	2008–2024	North	−5.68	[−7.98, −3.00]
Relative P90	2009–2024	East	−4.26	[−5.85, −2.70]
Relative P90	2009–2024	North	−4.56	[−6.76, −2.42]
Relative P80	2008–2024	East	−6.72	[−8.70, −4.14]
Relative P80	2008–2024	North	−7.16	[−9.29, −4.27]
Relative P95	2008–2024	East	−3.47	[−5.83, −1.22]
Relative P95	2008–2024	North	−4.97	[−7.72, −1.95]
Fixed P90	2008–2024	East	−1.00	[−5.46, 3.50]
Fixed P90	2008–2024	North	−0.27	[−4.56, 4.84]

Notes. East and north are the projected x and y coordinates of annual hotspot centroids in EPSG:6933; negative slopes indicate westward or southward change. Centroids use administrative overlap areas weighted by positive NH_3 excess above the specified threshold. The 95% intervals use paired three-year circular moving-block resampling of detrended coordinate residuals (1,999 replicates). Two-year block checks preserved the signs of relative-P80, P90 and P95 trends. The 2009–2024 rows exclude 2008. Endpoint distances are reported in Table S9B; fixed-P90 intervals include zero.

Table S11. Exact fitted configuration and implementation

Parameter	Value
model	UST-BART
implementation	XBART/GFR in StochTree 0.4.5
num_trees	100.00
num_gfr	80.00
discard_gfr	30.00
retained_gfr	50.00
num_burnin	0
num_mcmc	0
alpha	0.950
beta	2.00
max_depth	6.00
min_samples_leaf	20.00
cutpoint_grid_size	100.00
num_threads	4.00
seeds	[20261004, 20261005]
year_center	2015.00
province_encoding	Three binary one-hot columns, passed as ordered categorical levels [0,1]
likelihood	Gaussian
response_units	micromol/m2
uncertainty	approximate UST-BART GFR forest-response 95% bands; no calibrated MCMC claim
feature_order	["T2m between", "SM between", "BLH between", "AGS between", "MNM between", "SO_2 between", "NO_x between", "cropland_fraction between", "T2m within", "SM within", "BLH within", "AGS within", "MNM within", "SO_2 within", "NO_x within", "lon", "lat", "province_Liaoning", "province_Jilin", "province_Heilongjiang", "centered_year", "sin_month", "cos_month", "sin_month_2", "cos_month_2"]
num_burnin / num_mcmc	0 / 0

Parameter	Value
Response standardization	Training mean removed; divided by training population SD; predict restores original μmol m^{-2}
Leaf variance prior	Inverse-gamma(3, 0.01), sampled; standardized response
Global variance prior	Default shape 0, scale 0; limiting $1/\sigma^2$ prior
Province preprocessing	Three binary ordered categorical columns, levels [0,1]

The primary UST-BART specification and fitted forests are unchanged. Eighty GFR forests were saved; the first thirty are excluded from interpretation. Fifty remain per seed. No MCMC convergence or interval-calibration claim is made.

Table S12. Physical-driver model relevance

rank	Driver	overall relevance	overall lower95	overall upper95	between relevance	within relevance
1	T2m	32.21	30.75	33.64	2.18	30.04
2	BLH	22.23	21.14	23.33	1.42	20.82
3	SM	18.60	17.35	19.80	1.02	17.58
4	NH3-AGS	10.54	9.63	11.46	0.361	10.18
5	NH3-MNM	10.10	9.08	11.19	0.822	9.28
6	NOx	3.09	2.57	3.63	0.324	2.77
7	SO2	2.93	2.31	3.58	0.281	2.65
8	Cropland	0.290	0.096	0.576	0.290	0

All shares in %, normalized over physical splits only. Background splits are excluded. Overall = between + within. Bounds summarize retained forest split-use shares; this is not causal or explained-variance contribution.

Table S13A. Conditional-response support, direction and magnitude

Driver	Component	Predictor unit	P5	P95	Net change	Shape	Seed check
T2m	between	deg C	-0.912	9.70	8.49	monotonic-or-flat	STABLE
SM	between	m3/m3	0.250	0.364	-0.201	monotonic-or-flat / non-monotonic	UNSTABLE
BLH	between	m	479.88	606.36	-0.349	non-monotonic	MODERATE
NH3-AGS	between	kg/km2/year	5.73	3586.51	0.156	inverse-U / monotonic-or-flat	MODERATE
NH3-MNM	between	kg/km2/year	1.57	402.44	1.59	monotonic-or-flat	MODERATE
SO2	between	kg/km2/year	1.52	8102.02	0.511	monotonic-or-flat	MODERATE
NOx	between	kg/km2/year	10.16	8499.67	1.57	monotonic-or-flat	MODERATE
Cropland	between	fraction	0	0.984	0.596	monotonic-or-flat	MODERATE
T2m	within	deg C	-21.80	18.70	84.49	monotonic-or-flat	STABLE
SM	within	m3/m3	-0.063	0.057	-6.99	U-shape	STABLE
BLH	within	m	-253.86	315.82	10.22	inverse-U	STABLE
NH3-AGS	within	kg/km2/year	-407.64	370.62	-38.93	monotonic-or-flat	STABLE
NH3-MNM	within	kg/km2/year	-9.77	10.51	-5.44	U-shape	MODERATE
SO2	within	kg/km2/year	-561.13	549.97	-1.88	U-shape	STABLE
NOx	within	kg/km2/year	-388.38	370.03	-2.95	U-shape	STABLE

Endpoint changes in μmol m^{-2}, predictor bounds in their listed units. Inventories vary annually, meteorology monthly. Support covers P5–P95. Curves are independently centred.

Table S13B. Seed reproduction of physical responses

Driver	Component	Shape r	Endpoint sign	Slope agreement	Major turns	flattening	Seed check
T2m	between	0.978	Yes	1.00	Yes	Yes	STABLE
SM	between	0.202	No	0.615	No	Yes	UNSTABLE
BLH	between	0.840	Yes	0.667	Yes	Yes	MODERATE
NH3-AGS	between	0.981	Yes	0.737	No	Yes	MODERATE
NH3-MNM	between	0.972	Yes	0.556	Yes	Yes	MODERATE
SO2	between	0.959	Yes	0.353	Yes	Yes	MODERATE
NOx	between	0.998	Yes	0.667	Yes	Yes	MODERATE
Cropland	between	0.996	Yes	0.588	Yes	Yes	MODERATE
T2m	within	1.000	Yes	0.947	Yes	No	STABLE
SM	within	0.994	Yes	1.00	Yes	No	STABLE
BLH	within	0.999	Yes	1.00	Yes	No	STABLE
NH3-AGS	within	0.999	Yes	0.941	Yes	Yes	STABLE
NH3-MNM	within	0.995	Yes	0.789	Yes	Yes	MODERATE
SO2	within	0.997	Yes	0.947	Yes	Yes	STABLE
NOx	within	0.984	Yes	1.00	Yes	Yes	STABLE

These are computational reproduction diagnostics, not posterior-convergence tests. Major turns use prominence 20% of amplitude and ≥2 bins, matched within 15% of grid length.

Table S14A. Complete 105-pair screen

Pair	Role	Local RMS	Surface r	Supported fraction	Rectangles	Seed check
T2m W × BLH W	Main	25.02	0.978	1.00	25	STABLE
T2m W × SM W	Main	15.75	0.931	1.00	25	STABLE
T2m B × T2m W	Supplement	12.77	0.996	1.00	25	STABLE
T2m W × NH3-AGS W	Screen only	10.73	0.944	1.00	25	STABLE
T2m W × NH3-MNM W	Screen only	6.87	0.817	1.00	25	MODERATE
SM W × BLH W	Screen only	5.65	0.968	1.00	25	STABLE
BLH W × NH3-MNM W	Screen only	4.20	0.947	1.00	25	STABLE
T2m B × SM W	Screen only	3.46	0.989	1.00	25	STABLE
T2m W × SO2 W	Screen only	3.27	0.967	1.00	25	STABLE
BLH W × NH3-AGS W	Screen only	3.14	0.835	1.00	25	MODERATE
SM B × T2m W	Screen only	2.51	0.985	1.00	25	STABLE
NH3-MNM B × T2m W	Screen only	2.29	0.727	1.00	25	UNSTABLE
T2m W × NOx W	Screen only	1.97	0.876	1.00	25	MODERATE
T2m B × BLH W	Screen only	1.74	0.846	1.00	25	MODERATE
BLH B × T2m W	Screen only	1.43	0.894	1.00	25	MODERATE
SM W × NH3-MNM W	Screen only	1.46	0.786	1.00	25	UNSTABLE
SM B × BLH W	Screen only	1.08	0.959	1.00	25	UNSTABLE
SM W × NH3-AGS W	Screen only	1.25	0.864	1.00	25	MODERATE
NH3-MNM B × SM W	Screen only	0.821	0.967	1.00	25	STABLE
BLH W × NOx W	Screen only	0.993	0.832	1.00	25	MODERATE
T2m B × NH3-MNM B	Screen only	0.733	0.999	0.995	21	STABLE

Pair	Role	Local RMS	Surface r	Supported fraction	Rectangles	Seed check
NH3-AGS W × NH3-MNM W	Screen only	0.767	0.751	1.00	25	UNSTABLE
NH3-MNM B × BLH W	Screen only	0.592	0.800	1.00	25	MODERATE
BLH W × SO2 W	Screen only	0.605	0.766	1.00	25	UNSTABLE
SM W × NOx W	Screen only	0.508	0.867	1.00	25	MODERATE
BLH B × SM W	Screen only	0.549	0.746	1.00	25	UNSTABLE
NH3-AGS W × NOx W	Screen only	0.431	0.936	1.00	25	STABLE
T2m B × NH3-AGS W	Screen only	0.469	0.791	1.00	25	UNSTABLE
SM W × SO2 W	Screen only	0.456	0.755	1.00	25	UNSTABLE
BLH B × BLH W	Screen only	0.429	0.737	1.00	25	UNSTABLE
SM B × SM W	Screen only	0.408	0.753	1.00	25	UNSTABLE
T2m B × NH3-MNM W	Screen only	0.306	0.715	1.00	25	UNSTABLE
NH3-MNM W × NOx W	Screen only	0.237	0.908	1.00	25	MODERATE
SM B × NH3-AGS W	Screen only	0.170	0.960	0.999	24	UNSTABLE
NOx B × T2m W	Screen only	0.239	0.678	1.00	25	UNSTABLE
NH3-AGS B × T2m W	Screen only	0.272	0.555	1.00	25	UNSTABLE
NOx B × BLH W	Screen only	0.184	0.804	1.00	25	MODERATE
Cropland B × T2m W	Screen only	0.291	0.434	1.00	25	UNSTABLE
NH3-AGS B × NH3-AGS W	Screen only	0.179	0.706	1.000	19	UNSTABLE
SO2 B × SM W	Screen only	0.213	0.567	1.00	25	UNSTABLE
SO2 B × T2m W	Screen only	0.334	0.327	1.00	25	UNSTABLE
NH3-MNM B × NH3-AGS W	Screen only	0.134	0.792	1.00	25	UNSTABLE
NH3-AGS W × SO2 W	Screen only	0.191	0.498	1.00	25	UNSTABLE
SO2 W × NOx W	Screen only	0.165	0.542	1.00	25	UNSTABLE
SO2 B × NH3-AGS W	Screen only	0.105	0.799	1.00	25	UNSTABLE
NOx B × SM W	Screen only	0.156	0.527	1.00	25	UNSTABLE
SO2 B × BLH W	Screen only	0.125	0.640	1.00	25	UNSTABLE
T2m B × SO2 W	Screen only	0.074	0.744	1.00	25	UNSTABLE
BLH B × NH3-MNM W	Screen only	0.157	0.290	1.00	25	UNSTABLE
SM B × BLH B	Screen only	0.063	0.747	1.00	25	UNSTABLE
NH3-AGS B × BLH W	Screen only	0.115	0.356	1.00	25	UNSTABLE
NH3-AGS B × SM W	Screen only	0.167	0.231	1.00	25	UNSTABLE
BLH B × NOx W	Screen only	0.041	0.876	1.00	25	MODERATE
SM B × SO2 W	Screen only	0.045	0.748	1.00	25	UNSTABLE
NH3-AGS B × NH3-MNM W	Screen only	0.041	0.682	1.00	25	UNSTABLE
NOx B × NH3-AGS W	Screen only	0.023	0.972	1.000	24	UNSTABLE
NOx B × NH3-MNM W	Screen only	0.064	0.306	1.00	25	UNSTABLE
Cropland B × NH3-MNM W	Screen only	0.028	0.659	1.00	25	UNSTABLE
NH3-MNM B × SO2 W	Screen only	0.015	0.956	1.00	25	UNSTABLE
Cropland B × NH3-AGS W	Screen only	0.053	0.173	1.000	24	UNSTABLE
NH3-MNM B × NOx W	Screen only	0.024	0.225	1.00	25	UNSTABLE
SM B × NH3-MNM W	Screen only	0.090	0.037	1.00	25	UNSTABLE

Pair	Role	Local RMS	Surface r	Supported fraction	Rectangles	Seed check
SM B × NOx W	Screen only	0.020	0.126	1.00	25	UNSTABLE
SO2 B × NOx W	Screen only	0.010	0.042	1.00	25	UNSTABLE
NH3-AGS B × NH3-MNM B	Screen only	0.008	0.045	0.996	23	UNSTABLE
T2m B × BLH B	Screen only	0.000977	0	1.00	24	UNSTABLE
T2m B × SM B	Screen only	0.015	0	0.997	24	UNSTABLE
BLH B × NH3-MNM B	Screen only	0.008	0	0.995	24	UNSTABLE
SM B × NH3-MNM B	Screen only	1.66e-17	0	1.00	25	UNSTABLE
NOx B × NOx W	Screen only	0.010	0	0.999	23	UNSTABLE
NOx B × SO2 W	Screen only	1.28e-17	0	0.999	24	UNSTABLE
Cropland B × SO2 W	Screen only	4.41e-17	0	1.00	25	UNSTABLE
Cropland B × NOx W	Screen only	0.003	0	1.00	25	UNSTABLE
SO2 B × SO2 W	Screen only	0.000782	0	1.000	22	UNSTABLE
T2m B × SO2 B	Screen only	0.014	0	0.996	24	UNSTABLE
T2m B × Cropland B	Screen only	0.011	0	1.00	25	UNSTABLE
BLH B × NH3-AGS B	Screen only	0.025	0	1.00	25	UNSTABLE
BLH B × Cropland B	Screen only	0.050	0	1.00	25	UNSTABLE
BLH B × NOx B	Screen only	0.011	0	1.00	25	UNSTABLE
SM B × NH3-AGS B	Screen only	0.013	0	0.989	21	UNSTABLE
BLH B × SO2 B	Screen only	1.68e-18	0	1.00	25	UNSTABLE
SM B × Cropland B	Screen only	1.73e-18	0	0.997	23	UNSTABLE
SM B × SO2 B	Screen only	0.006	0	0.996	24	UNSTABLE
SM B × NOx B	Screen only	6.8e-18	0	0.999	24	UNSTABLE
NH3-MNM B × NOx B	Screen only	0.002	0	1.00	25	UNSTABLE
NH3-MNM B × Cropland B	Screen only	0.016	0	1.00	25	UNSTABLE
NH3-AGS B × Cropland B	Screen only	0	0	0.993	20	UNSTABLE
NH3-AGS B × NOx B	Screen only	0	0	0.995	21	UNSTABLE
NOx B × Cropland B	Screen only	1.22e-17	0	0.998	23	UNSTABLE
NH3-AGS B × SO2 B	Screen only	1.18e-18	0	0.992	22	UNSTABLE
SO2 B × Cropland B	Screen only	1.56e-17	0	0.993	23	UNSTABLE
T2m B × NOx B	Screen only	0.004	-0.060	1.00	25	UNSTABLE
NH3-AGS B × NOx W	Screen only	0.011	-0.042	1.00	25	UNSTABLE
SO2 B × NOx B	Screen only	0.011	-0.059	0.992	18	UNSTABLE
NH3-AGS B × SO2 W	Screen only	0.023	-0.028	1.00	25	UNSTABLE
NH3-MNM B × SO2 B	Screen only	0.026	-0.045	0.995	23	UNSTABLE
T2m B × NH3-AGS B	Screen only	0.032	-0.052	0.997	24	UNSTABLE
T2m B × NOx W	Screen only	0.028	-0.194	1.00	25	UNSTABLE
SO2 B × NH3-MNM W	Screen only	0.016	-0.374	1.00	25	UNSTABLE
BLH B × SO2 W	Screen only	0.006	-0.978	1.00	25	UNSTABLE
Cropland B × BLH W	Screen only	0.027	-0.266	1.00	25	UNSTABLE
NH3-MNM B × NH3-MNM W	Screen only	0.024	-0.711	1.000	24	UNSTABLE
BLH B × NH3-AGS W	Screen only	0.028	-0.626	1.00	25	UNSTABLE

Pair	Role	Local RMS	Surface r	Supported fraction	Rectangles	Seed check
NH3-MNM W × SO2 W	Screen only	0.057	-0.436	1.00	25	UNSTABLE
Cropland B × SM W	Screen only	0.046	-0.618	1.00	25	UNSTABLE

B = between, W = within. RMS in μmol m⁻²; support fraction and r dimensionless. All pairs remain visible, including weak/unsupported results. Co-occurrence only screens candidates. This table does not apply a 105-pair inferential significance threshold.

Table S14B. Principal local rectangles and observed support

a	b	a lo	a hi	b lo	b hi	Rows	Locations
8	10	9.24	14.16	-33.85	24.47	11,302	2,263
8	9	14.16	18.70	-0.026	-0.006	7,805	2,202

Index 8 = T within (°C), 9 = SM within (m³ m⁻³), 10 = BLH within (m). One observed context per selected location, at most 24 locations; identical references across seeds. Contrast/bounds in μmol m⁻², pointwise only.

Table S14B. Principal local rectangles and observed support (continued measures)

a	b	References	contrast	Lower band	Upper band
8	10	24	64.41	22.99	96.73
8	9	24	-41.94	-78.30	-6.13

Index 8 = T within (°C), 9 = SM within (m³ m⁻³), 10 = BLH within (m). One observed context per selected location, at most 24 locations; identical references across seeds. Contrast/bounds in μmol m⁻², pointwise only.

Table S15. Province-specific net response changes

Driver	Province	Common low	Common high	Net response	Lower band	Upper band	Seed r
T2m	Liaoning	-18.42	15.85	234.40	163.80	286.70	1.000
T2m	Jilin	-18.42	15.85	133.47	87.78	176.01	0.999
T2m	Heilongjiang	-18.42	15.85	53.16	19.55	82.90	0.985
SM	Liaoning	-0.059	0.050	-13.71	-33.66	6.69	0.997
SM	Jilin	-0.059	0.050	4.09	-8.92	14.84	0.943
SM	Heilongjiang	-0.059	0.050	-5.24	-14.16	3.93	0.984
BLH	Liaoning	-187.73	249.59	-12.39	-40.20	16.21	0.990
BLH	Jilin	-187.73	249.59	45.00	27.30	62.62	0.996
BLH	Heilongjiang	-187.73	249.59	8.10	-10.55	27.41	0.994
NH3-AGS	Liaoning	-383.06	334.32	-65.66	-83.39	-51.23	1.000
NH3-AGS	Jilin	-383.06	334.32	-34.24	-42.88	-24.24	1.000
NH3-AGS	Heilongjiang	-383.06	334.32	-21.23	-30.03	-14.02	0.999

Common-range changes and bounds in μmol m⁻²; predictor ranges in Table 1 units. Province curves use their own reference contexts and centring. Changes are across the entire shared range, not per-unit effects.

Table S16A. Group-specific held-out bias

split	Group	Level	N	Mean bias	Observed mean	Predicted mean
temporal	overall	all	96,379	2.09	116.77	118.86
spatial	overall	all	70,797	0.961	81.14	82.10
temporal	month	1	6,676	-0.552	46.58	46.03
temporal	month	2	7,246	-9.59	56.42	46.83
temporal	month	3	8,335	-15.90	80.99	65.09
temporal	month	4	8,686	-20.23	105.85	85.62
temporal	month	5	8,730	-16.41	154.95	138.53

split	Group	Level	N	Mean bias	Observed mean	Predicted mean
temporal	month	6	8,554	27.48	217.25	244.73
temporal	month	7	8,770	5.66	253.31	258.97
temporal	month	8	8,204	27.14	133.08	160.22
temporal	month	9	8,446	33.07	106.18	139.25
temporal	month	10	8,556	-3.31	81.26	77.95
temporal	month	11	7,492	0.981	61.00	61.98
temporal	month	12	6,684	-5.97	54.87	48.91
temporal	province	Heilongjiang	54,013	4.84	87.40	92.24
temporal	province	Jilin	23,608	-1.03	122.86	121.83
temporal	province	Liaoning	18,758	-1.91	193.70	191.79
temporal	year	2019	24,213	20.83	106.62	127.45
temporal	year	2020	23,812	17.42	109.28	126.69
temporal	year	2021	24,182	-19.35	131.47	112.11
temporal	year	2022	24,172	-10.34	119.63	109.28
spatial	month	1	4,616	-3.45	52.37	48.91
spatial	month	2	4,902	2.06	45.36	47.42
spatial	month	3	5,815	7.09	40.35	47.44
spatial	month	4	6,643	7.28	65.01	72.29
spatial	month	5	6,763	-3.77	97.47	93.70
spatial	month	6	6,823	-43.81	184.41	140.60
spatial	month	7	6,519	15.51	142.89	158.40
spatial	month	8	5,994	27.24	74.78	102.02
spatial	month	9	6,399	7.87	62.21	70.08
spatial	month	10	6,554	1.84	64.02	65.86
spatial	month	11	5,353	0.402	49.16	49.56
spatial	month	12	4,416	-4.60	53.50	48.90
spatial	province	Heilongjiang	64,056	0.666	81.89	82.56
spatial	province	Jilin	6,741	3.76	74.04	77.81
spatial	year	2008	4,841	5.87	72.44	78.31
spatial	year	2009	4,590	2.15	64.85	67.00
spatial	year	2010	4,508	-0.144	71.46	71.32
spatial	year	2011	4,684	7.73	64.52	72.25
spatial	year	2012	4,601	0.663	67.56	68.23
spatial	year	2013	4,429	5.63	65.69	71.32
spatial	year	2014	4,707	-8.85	89.91	81.07
spatial	year	2015	4,750	-4.21	84.64	80.43
spatial	year	2016	4,721	-14.67	92.01	77.34
spatial	year	2017	4,723	3.29	85.86	89.16
spatial	year	2018	4,847	5.93	99.01	104.94
spatial	year	2019	4,940	-2.40	89.86	87.46
spatial	year	2020	4,747	9.97	76.69	86.66

split	Group	Level	N	Mean bias	Observed mean	Predicted mean
spatial	year	2021	4,844	-5.47	101.94	96.48
spatial	year	2022	4,865	9.00	87.02	96.02

All means and biases in μmol m^{-2}. Bias = predicted − observed. Overall metrics are in Table 2A; temporal/spatial background comparator uses the same partitions.

Table S16B. Independent validation recomputation and baseline

Model	Holdout	RMSE	MAE	R^2	Mean bias	Moran's I
UST-BART	Temporal	87.25	56.28	0.414	2.09	0.717
Background-only XBART	Temporal	109.56	71.86	0.075	-21.85	—
UST-BART	Spatial	69.34	44.22	0.286	0.961	0.493
Background-only XBART	Spatial	82.87	54.38	-0.020	-1.22	—

Metrics and units follow Table 2A. Spatial validation covers eastern Jilin and Heilongjiang and does not separately validate Liaoning extrapolation.

Table S17. Matched-holdout comparison of decomposed and undecomposed predictor specifications

Holdout	Specification	N	RMSE	MAE	R^2	Bias
Temporal	UST-BART	96,379	87.25	56.28	0.414	+2.09
Temporal	Undecomposed	96,379	81.24	52.42	0.492	-19.82
Spatial	UST-BART	70,797	69.34	44.22	0.286	+0.96
Spatial	Undecomposed	70,797	73.13	45.87	0.206	-0.94

Notes. Both models were trained and evaluated on identical nonnegative observations and temporal/spatial holdout partitions. The frozen UST-BART uses 25 inputs (seven location means, seven within-location departures, cropland and ten background variables) and predictions pooled from two seeds. The undecomposed XBART uses 18 inputs (seven original dynamic predictors, cropland and the same ten background variables), with unchanged GFR settings and seed 20261004. All errors and biases are in μmol m^{-2}; bias = predicted − observed. This is a fixed-seed model-specification comparison, not evidence of universal predictive superiority.

An auxiliary response-selection fit retained finite signed NH_3 retrievals and complete predictors (N = 409,286), including 54,747 negative estimates. It used the primary model's 25 inputs, GFR settings and holdout definitions with seed 20261004. The frozen primary two-seed predictions and the auxiliary fit were compared only on matched nonnegative holdout rows; low-column strata were defined by the observed P10 threshold within each holdout (Table S18). Negative retrieval estimates were not interpreted as physically negative atmospheric columns. This single-seed auxiliary fit serves as a targeted sensitivity check rather than a refit of the primary ensemble.

Table S18A. Low-column response-selection sensitivity

Matched nonnegative holdout observations in the lowest decile of the observed NH_3 column. All errors and P10 thresholds in μmol m^{-2}. Bias = predicted minus observed.

Holdout	Model fitted on	N	P10 cutoff	Bias	RMSE	MAE
Temporal	nonnegative	9,638	17.86	49.32	59.58	49.37
Temporal	signed	9,638	17.86	35.21	51.61	35.43
Spatial	nonnegative	7,080	13.74	51.76	58.11	51.76
Spatial	signed	7,080	13.74	36.38	47.25	36.38

The P10 thresholds are defined from observed nonnegative test responses within each holdout, and the comparison uses the same nonnegative test rows for both fits. The signed estimates are retrieval outputs, not physically negative atmospheric columns.

Table S18B. Overall matched-holdout performance

Full matched nonnegative test sets. Bias, RMSE and MAE in μmol m^{-2}.

Holdout	Model fitted on	N	Bias	RMSE	MAE	R^2
Temporal	nonnegative	96,379	2.09	87.25	56.28	0.414
Temporal	signed	96,379	-6.28	87.78	56.38	0.406
Spatial	nonnegative	70,797	0.960	69.34	44.22	0.286
Spatial	signed	70,797	-10.94	70.96	44.09	0.252

Model fitted on nonnegative = original frozen two-seed UST-BART ensemble; model fitted on signed = one-seed auxiliary UST-BART fit retaining finite negative retrievals. Different training response support is the intended sensitivity; overall matched tests are strictly identical.

Table S19A. Core ALE sample-split reproduction

Component	seed	Half-shape r	Max lower-edge Δ	Max upper-edge Δ	Curve amplitude
T2m between	seed1	0.999	2.77	1.43	8.49
T2m between	seed2	0.998	0.756	1.12	8.49
T2m within	seed1	0.995	9.96	6.38	87.43
T2m within	seed2	0.998	11.18	9.73	87.43
SM within	seed1	0.995	3.29	1.46	12.94
SM within	seed2	0.987	2.96	3.38	12.94
BLH within	seed1	0.994	5.26	4.86	32.40
BLH within	seed2	0.994	9.66	2.13	32.40

Each retained run is split into consecutive 25/25 forests. Band-edge differences and amplitudes in μmol m^{-2}. Mean-shape correlation is a reproduction check; endpoints are approximate and not calibrated observation intervals.

Table S19B. Paired province temperature net changes

province a	province b	common low	common high	Mean difference	Lower band	Upper band
Liaoning	Jilin	-18.42	15.85	100.93	26.14	169.17
Liaoning	Heilongjiang	-18.42	15.85	181.24	106.61	242.99
Jilin	Heilongjiang	-18.42	15.85	80.30	23.56	125.38

Common predictor range in °C; differences and pointwise approximate bands in μmol m^{-2}. Paired differences use identical forests and province-specific observed contexts.

Table S19C. Principal local contrast sample-split bands

a	b	contrast	Half 1 lower	Half 1 upper	Half 2 lower	Half 2 upper
8	10	64.41	19.20	89.18	38.96	101.43
8	9	-41.94	-70.92	-1.95	-78.79	-12.59

Each pooled half contains 25 forests from each seed. All contrasts/bounds in μmol m^{-2}. Index definitions follow Table S14B. Pointwise bands support a local, not simultaneous, comparison.

References

Apley, D.W.; Zhu, J. (2020). Visualizing the effects of predictor variables in black box supervised learning models. Journal of the Royal Statistical Society: Series B, 82, 1059–1086. https://doi.org/10.1111/rssb.12377

Benjamini, Y.; Hochberg, Y. (1995). Controlling the false discovery rate: A practical and powerful approach to multiple testing. Journal of the Royal Statistical Society: Series B, 57, 289–300. https://doi.org/10.1111/j.2517-6161.1995.tb02031.x

Chipman, H.A.; George, E.I.; McCulloch, R.E. (2010). BART: Bayesian additive regression trees. The Annals of Applied Statistics, 4, 266–298. https://doi.org/10.1214/09-AOAS285

Clarisse, L.; Franco, B.; Van Damme, M.; Di Gioacchino, T.; Hadji-Lazaro, J.; Whitburn, S.; Noppen, L.; Hurtmans, D.; Clerbaux, C.; Coheur, P. (2023). The IASI NH_3 version 4 product: Averaging kernels and improved consistency. Atmospheric Measurement Techniques, 16, 5009–5028. https://doi.org/10.5194/amt-16-5009-2023

Curran, P.J.; Bauer, D.J. (2011). The disaggregation of within-person and between-person effects in longitudinal models of change. Annual Review of Psychology, 62, 583–619. https://doi.org/10.1146/annurev.psych.093008.100356

ECMWF (n.d.-a). ERA5 monthly averaged data on single levels. Climate Data Store. https://cds.climate.copernicus.eu/datasets/reanalysis-era5-single-levels-monthly-means (accessed 11 October 2026).

ECMWF (n.d.-b). ERA5-Land monthly averaged data. Climate Data Store. https://cds.climate.copernicus.eu/datasets/reanalysis-era5-land-monthly-means (accessed 11 October 2026).

ESA Climate Change Initiative (2026). IASI NH_3 Level-3 MERGED product, version 4.0.1R. CEDA Archive. https://catalogue.ceda.ac.uk/uuid/2ec5b1fb653445bdbbd0dcd69dd223da/ (accessed 11 October 2026).

ESA Climate Change Initiative (2024). Precursors Product User Guide, D4.2, version 01_01. https://climate.esa.int/documents/2636/Precursors_cci_D4.2_PUG_01_01.pdf (accessed 11 October 2026).

European Commission, Joint Research Centre (n.d.). EDGAR v8.1 FT2022 air pollutants. https://edgar.jrc.ec.europa.eu/dataset_ap81 (accessed 11 October 2026).

geoBoundaries (2023). gbOpen CHN ADM1, boundary ID CHN-ADM1-43563684, reference year 2019; pinned repository revision 9469f09. https://www.geoboundaries.org/api/current/gbOpen/CHN/ADM1/ (accessed 11 October 2026).

He, J.; Yalov, S.; Hahn, P.R. (2019). XBART: Accelerated Bayesian Additive Regression Trees. Proceedings of Machine Learning Research, 89, 1130–1138. https://proceedings.mlr.press/v89/he19a.html

Mann, H.B. (1945). Nonparametric tests against trend. Econometrica, 13, 245–259. https://doi.org/10.2307/1907187

Newey, W.K.; West, K.D. (1987). A simple, positive semi-definite, heteroskedasticity and autocorrelation consistent covariance matrix. Econometrica, 55, 703–708. https://doi.org/10.2307/1913610

Sen, P.K. (1968). Estimates of the regression coefficient based on Kendall's tau. Journal of the American Statistical Association, 63, 1379–1389. https://doi.org/10.1080/01621459.1968.10480934

StochTree (2026). Supervised learning in StochTree. Installed Python implementation version 0.4.5; general model and sampler documentation. https://stochtree.ai/about/bart.html (accessed 11 October 2026).

Sulla-Menashe, D.; Friedl, M.A. (2022). User Guide to Collection 6.1 MODIS Land Cover (MCD12Q1 and MCD12C1). https://lpdaac.usgs.gov/documents/1409/MCD12_User_Guide_V61.pdf (accessed 11 October 2026).